

An interpretable probabilistic machine learning method for heterogeneous longitudinal studies

Juho Timonen, Henrik Mannerström, Aki Vehtari and Harri Lähdesmäki*
Department of Computer Science, Aalto University

October 31, 2021

Abstract

Identifying risk factors from longitudinal data requires statistical tools that are not restricted to linear models, yet provide interpretable associations between different types of covariates and a response variable. Here, we present a widely applicable and interpretable probabilistic machine learning method for nonparametric longitudinal data analysis using additive Gaussian process regression. We demonstrate that it outperforms previous longitudinal modeling approaches and provides useful novel features, including the ability to account for uncertainty in disease effect times as well as heterogeneity in their effects.

Background

Biological and medical studies often collect observational longitudinal data, where repeated measurements of the same individuals are made at several time points. This is an indispensable study design for examining disease development and other temporal phenomena, and has been leveraged for example in proteomics [1], metagenomics [2, 3], other -omics studies and even single-cell transcriptomics [4, 5]. The measured response variable of interest can be continuous (such as abundance of a protein), discrete (such as number of methylated reads at a certain position), or binary (such as patient condition). Often also a number of explanatory variables – or covariates – are measured for each subject and measurement time point. These can be categorical variables (such as sex, location or whether the subject is diagnosed with a disease or not) or continuous (such as age, time from disease initiation or blood pressure) and inferring which covariates affect the response variable, or are potential risk factors, is a medically motivated question. A large body of literature has focused on statistical analysis of lon-

gitudinal data [6], for the purposes of temporal trend analysis, predictive modeling or studying covariate effects. Observations of one individual are intercorrelated, and specialized statistical techniques are therefore required to draw sensible conclusions. Generalized linear mixed (GLM) models [7], which contain both fixed and random effects, have become the standard workhorse for longitudinal data analysis due to their general applicability, ease of use, interpretability and software support. The R package *lme4* [8] has gained high popularity and become a default choice for fitting GLM models. These models, however, require specifying a parametric (linear) form for the covariate effects, and provide biased inferences when their true effects are nonlinear. Moreover, GLM models cannot capture nonstationary effects that can occur rapidly e.g. near the disease initiation time. See Supplementary material for more background information and related research.

Results and discussion

In this work we propose a Bayesian nonparametric method, *lgpr*, for modeling longitudinal data

*corresponding author

using additive Gaussian processes (GPs) [9]. It is designed for accurate and interpretable learning of possibly nonlinear or nonstationary effects of individual covariates or their interactions. We demonstrate that our method significantly improves previous longitudinal analysis methods and provides novel features to the longitudinal modeling toolkit: *lgpr* supports non-Gaussian observation models, includes kernels for interpretable modeling of various types of covariate effects, unique features that can identify heterogeneous biomarkers that are detectable only in a subset of patients, and a possibility to model uncertainty in disease effect times. Furthermore, *lgpr* can compute covariate relevances for different types of covariates, and perform accurate covariate selection. We have implemented *lgpr* as an R package [10] that can be used as a plug-in replacement for *lme4*. The new tool is summarized in Figure 1a.

In our approach, we use GPs to model the longitudinal response y in a Bayesian manner by defining a prior directly for the underlying unknown signal f , which is linked to y through a likelihood function, which is motivated by the statistical observation model. Properties of a GP are defined by its kernel function $k(\mathbf{x}, \mathbf{x}')$, which encodes the covariance of function values at different input points. Additive GPs assume that the signal (or equivalently the kernel) is additive, $f = f^{(1)}(\mathbf{x}) + \dots + f^{(J)}(\mathbf{x})$, and *lgpr* specifically assumes that each $f^{(j)}$ depends only on a single covariate or a pair of covariates (Figure 1b-c). For example, for a model with age and sex as covariates, *lgpr* can model the signal as $f = f^{(1)}(\text{age}) + f^{(2)}(\text{sex}, \text{age})$, where the first component represents a shared age effect and the second represents sex-specific deviation from it. This additive model structure allows one to define appropriate kernels for different covariates (discrete, continuous or interaction), and to retrieve interpretable covariate effects after model fitting. For components like $f^{(2)}$, we use a zero-sum kernel (Supplementary material: Figure S1) which is similar to the kernel used in [11] and allows GP modeling that separates shared and category-specific effects.

Parameters of an *lgpr* model include parameters of the observation model and the kernel (hyper)parameters, among others, and they are assigned robust priors that regularize model fitting

(Supplementary material: Figure S2). Bayesian model inference is carried out using the dynamic Hamiltonian Monte Carlo sampler [12, 13], as implemented in the high-performance statistical computation framework Stan [14]. We develop a rigorous and interpretable probabilistic covariate selection method which is based on fitting only one model with all covariates and estimating the proportion of variance explained by each signal component and noise. A detailed description of the modeling and inference methodology is given in Supplementary material. Using simulated data, we show that *lgpr* results in better covariate selection accuracy than linear mixed modeling with significance testing (Figure 2a, Supplementary material: Figure S3a) and an earlier Gaussian process regression method *LonGP* [15] (Supplementary material: Figure S3b).

Due to computational convenience, GP regression usually assumes a continuous Gaussian observation model, which is not statistically appropriate when modeling discrete count data as commonly produced in -omics studies. A common approach is to use the Gaussian observation model after first applying a variance-stabilizing transform, such as log-transform, to the response variable, but this is not statistically justified and can lead to biased inferences [16]. As a notable extension to existing literature, our package implements additive GP modeling and covariate selection also in the case of a non-Gaussian observation model (Supplementary material). We have implemented exact inference under the Poisson, Bernoulli, binomial and negative binomial (NB) observation model, and extending the *lgpr* tool with other observation models is straightforward. We use simulated longitudinal count data to show that using a negative binomial observation model gives better covariate selection accuracy than Gaussian observation model with or without log-transforming the counts (Figure 2b).

Longitudinal studies often comprise a case and control group, and it is common that a clinically determined time of disease initiation for each case individual is marked in the data. In order to reveal phenomena related to disease progression or to identify biomarkers, statistical modeling can utilize the disease-related age, i.e. time from disease initiation or onset, as one covariate that can explain changes in the response variable. Disease ef-

fects can be rapid when compared to other effects and expected to occur near the time of disease initiation, and which is why a nonstationary GP kernel is justified for the disease-related age. This approach was used in [15]. We propose a new variance masking kernel for more interpretable modeling of non-stationary disease effects (Supplementary material: Figure S4). The proposed approach separates the effect caused by the disease initiation from a possible baseline difference between cases and controls.

An inherent problem that can confound the analysis of disease effects, is that the disease initiation (or onset) time is difficult to determine exactly. For example in Type 1 Diabetes (T1D), the presence of islet cell autoantibodies in the blood is the earliest known marker of disease initiation [17], but they can only be measured when the subject visits a doctor. In general, the detected disease initiation time can differ from the true initiation time, and the magnitude of this difference can vary across individuals and response variables. Our tool can account for uncertainty in the disease effect time, and provides an option for the user to set a prior for the effect times globally or relative to the clinically determined onset or initiation time. This important feature could even reveal previously unknown biomarkers, which, at a younger age than known markers, predict the risk of developing a disease. Using simulated data, we show that modeling the effect time uncertainty improves the accuracy of detecting the disease effect (Figure 2c, Supplementary material: Figures S5-S6).

Another challenge in biomedical studies is that many diseases, such as T1D, are heterogeneous [18], and disease-specific biomarkers are likely to be detectable in only a subset of the diagnosed individuals. Our package also includes unique features for modeling heterogeneous disease effects. The disease effect size is allowed to vary between individuals, yet the statistical power from all diagnosed subjects is utilized (Supplementary material: Figure S4). Using simulated data, we show that if the real effect is not present for all diagnosed individuals, the heterogeneous modeling approach improves covariate selection accuracy (Figure 2d, Supplementary material: Figures S7-S8). Furthermore, the inference results provide information about which case subjects are affected by

the disease (Figure 2e,g,l, Supplementary material: Figure S7).

We used *lgpr* to analyze a longitudinal data set from a recent T1D study [1], where the longitudinal profile of plasma proteins was measured from 11 cases and 10 controls at nine time points that span the initiation of the disease pathogenesis. We performed the analysis for 1538 proteins separately, using both the homogeneous and heterogeneous disease effect modeling approach. In total, the homogeneous model finds 38 and the heterogeneous model finds 66 proteins associated with the disease-related age covariate, with intersection of 20 proteins. Covariate selection results for all proteins are included in Supplementary Tables S1-S2. Figure 2f shows the normalized measurements for Protein Q8WA1 (*O-linked-mannose beta-1,2-N-acetylglucosaminyltransferase 1*) and Figures 2h-i show the inferred covariate effects using two different disease effect modeling approaches. The new heterogeneous modeling approach is seen to detect a stronger average disease effect, because it allows the effect sizes to vary between individuals. Moreover, the posterior distributions of individual-specific disease effect magnitude parameters (Figure 2l), reveal four individuals ($id = 15, 16, 17, 21$) (Figure 2g), that experience a strong disease effect near the sero-conversion time.

Conclusions

The *lgpr* tool provides several important novel features for modeling longitudinal data, and offers a good balance between flexibility and interpretability. We have shown that the interpretable kernels, heterogeneous disease modeling, uncertainty modeling of effect times, and covariate selection strategy of *lgpr* significantly improve previous longitudinal modeling methods. The tool has an intuitive syntax, and thus provides an easy transition from the standard tools to Bayesian non-parametric longitudinal regression. It is generally applicable as the data can involve irregular sampling intervals or different number of measurement points over individuals and enjoys state-of-the art posterior sampling efficiency and diagnostics [19] offered by Stan. Moreover, many types of response variables that are common in postgenomic studies (continuous, discrete, binary, proportion) can

be modeled with the proper observation model. The user can choose from the numerous presented modeling options and set various parameter priors (which have widely applicable defaults). Overall, *lgpr* has potential to become a standard tool for statistical analysis of longitudinal data.

Methods

See Supplementary material for full description of the used methodology.

Authors' contributions

HL conceived the study. JT and HL designed the models and experiments with the help of AV. HM composed and derived the zero-sum kernel. JT developed the *lgpr* software and carried out the experiments. JT and HL wrote the manuscript with contributions from all authors. All authors read and approved the final manuscript.

Funding

This work has been supported by the Academy of Finland grant no. 292660.

Acknowledgements

The authors acknowledge the computational resources provided by the Aalto Science-IT project.

Availability of data and materials

The longitudinal proteomics data analyzed in this study can be found online at <https://doi.org/10.1016/j.jprot.2017.10.004> (raw data) and <https://github.com/jtimonen/lgpr-usage> (preprocessed data). The home page of the *lgpr* software is at <https://jtimonen.github.io/lgpr-usage/index.html>, and it contains installation instructions, tutorials, package manual, and code for reproducing the experiments of this manuscript. A static version of the R package source code is available at <http://doi.org/10.5281/zenodo.3563476>. The software supports all major operating systems, requires R version 3.4.0 or later and is licensed under the GPL 3 license.

Supplementary material

Detailed description of methods and experiments. Overview of related research. Supplementary Figures S1-S8. Supplementary Tables S1-S2.

References

- [1] C.-W. Liu, L. Bramer, B.-J. Webb-Robertson, K. Waugh, M. J. Rewers, and Q. Zhang, "Temporal expression profiling of plasma proteins reveals oxidative stress in early stages of type 1 diabetes progression," *Journal of Proteomics*, vol. 172, pp. 100–110, 2018.
- [2] T. Vatanen, A. Kostic, E. d'Hennezel, H. Siljander, E. A. Franzosa, M. Yassour, R. Kolde, H. Vlamakis, T. D. Arthur, A.-M. Hämäläinen, A. Peet, V. Tillmann, R. Uibo, S. Mokurov, N. Dorshakova, J. Ilonen, S. M. Virtanen, S. J. Szabo, J. A. Porter, and R. J. Xavier, "Variation in microbiome LPS immunogenicity contributes to autoimmunity in humans," *Cell*, vol. 165, 04 2016.
- [3] C. Stewart, N. J. Ajami, J. O'Brien, D. Hutchinson, D. Smith, M. Wong, M. Ross, R. Lloyd, H. Doddapaneni, G. Metcalf, D. Muzny, R. Gibbs, T. Vatanen, C. Huttenhower, R. Xavier, M. Rewers, W. Hagopian, J. Toppari, A.-G. Ziegler, and J. Petrosino, "Temporal development of the gut microbiome in early childhood from the TEDDY study," *Nature*, vol. 562, pp. 583–588, 10 2018.
- [4] A. Sharma, E. Cao, V. Kumar, X. Zhang, H.-S. Leong, A. Wong, N. Ramakrishnan, M. Hakimullah, H. Teo, F. Chong, S. Chia, M. Thangavelu, X. Kwang, R. Gupta, J. Clark, G. Periyasamy, N. G. Iyer, and R. Dasgupta, "Longitudinal single-cell RNA sequencing of patient-derived primary cells reveals drug-induced infidelity in stem cell hierarchy," *Nature Communications*, vol. 9, 12 2018.
- [5] M. Strunz, L. M. Simon, M. Ansari, L. F. Mattner, I. Angelidis, C. H. Mayr, J. Kathiriya, M. Yee, P. Ogar, A. Sengupta, I. Kukhtevich, R. Schneider, Z. Zhao, J. H. Neumann, J. Behr, C. Voss, T. Stöger, M. Lehmann, M. Königshoff, G. Burgstaller, M. O'Reilly, H. A. Chapman, F. J. Theis, and H. B. Schiller, "Longitudinal single cell transcriptomics reveals Krt8+ alveolar epithelial progenitors in lung regeneration," *bioRxiv*, DOI: 10.1101/705244, 2019.
- [6] P. Diggle, P. Heagerty, K.-Y. Liang, and S. Zeger, *Analysis of Longitudinal Data*. United Kingdom: Oxford University Press, 2002.
- [7] W. W. Stroup, *Generalized Linear Mixed Models: Modern Concepts, Methods and Applications*. Chapman & Hall/CRC Texts in Statistical Science, Boca Raton, Florida: CRC Press, 2012.
- [8] D. Bates, M. Mächler, B. Bolker, and S. Walker, "Fitting linear mixed-effects models using lme4,"

- Journal of Statistical Software*, vol. 67, no. 1, pp. 1–48, 2015.
- [9] C. E. Rasmussen and C. K. I. Williams, *Gaussian Processes for Machine Learning*. Cambridge, Massachusetts: MIT Press, 2006.
- [10] R Core Team, *R: A Language and Environment for Statistical Computing*. R Foundation for Statistical Computing, Vienna, Austria, 2018.
- [11] C. G. Kaufman and S. R. Sain, “Bayesian functional ANOVA modeling using Gaussian process prior distributions,” *Bayesian Analysis*, vol. 5, no. 1, pp. 123–149, 2010.
- [12] M. D. Hoffman and A. Gelman, “The No-U-Turn Sampler: Adaptively setting path lengths in Hamiltonian Monte Carlo,” *Journal of Machine Learning Research*, vol. 15, no. 1, pp. 1593–1623, 2014.
- [13] M. Betancourt, “A conceptual introduction to Hamiltonian Monte Carlo,” *arXiv:1701.02434*, 2017.
- [14] B. Carpenter, A. Gelman, M. D. Hoffman, D. Lee, B. Goodrich, M. Betancourt, M. A. Brubaker, J. Guo, P. Li, and A. Riddell, “Stan: A probabilistic programming language,” *Journal of Statistical Software*, vol. 76, no. 1, 2017.
- [15] L. Cheng, S. Ramchandran, T. Vatanen, N. Lietzen, R. Lahesmaa, A. Vehtari, and H. Lähdesmäki, “An additive Gaussian process regression model for interpretable non-parametric analysis of longitudinal data,” *Nature Communications*, vol. 10, no. 1, 2019.
- [16] R. B. O’Hara and D. J. Kotze, “Do not log-transform count data,” *Methods in Ecology and Evolution*, vol. 1, no. 2, pp. 118–122, 2010.
- [17] A. G. Ziegler, M. Rewers, O. Simell, T. Simell, J. Lempainen, A. Steck, C. Winkler, J. Ilonen, R. Veijola, M. Knip, E. Bonifacio, and G. S. Eisenbarth, “Seroconversion to Multiple Islet Autoantibodies and Risk of Progression to Diabetes in Children,” *JAMA*, vol. 309, no. 23, pp. 2473–2479, 2013.
- [18] M. Pietropaolo, E. Barinas-Mitchell, and L. H. Kuller, “The heterogeneity of diabetes,” *Diabetes*, vol. 56, no. 5, pp. 1189–1197, 2007.
- [19] A. Vehtari, A. Gelman, D. Simpson, B. Carpenter, and P.-C. Bürkner, “Rank-normalization, folding, and localization: An improved \hat{R} for assessing convergence of MCMC,” *arXiv:1903.08008*, 2019.

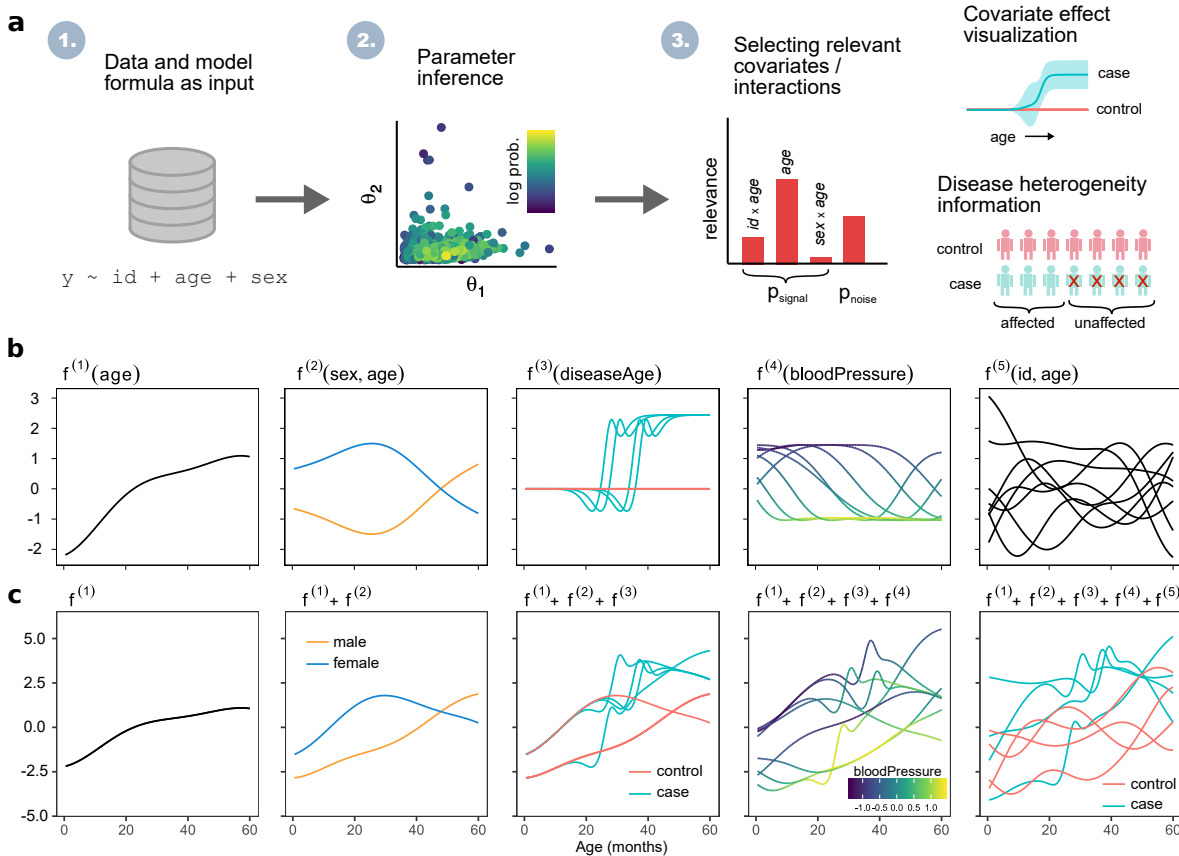


Figure 1 | Overview of additive Gaussian process modeling of longitudinal data using *lgpr*. a) A typical workflow with *lgpr*. 1. User gives the data and model formula as input, along with possible additional modeling options such as non-default parameter priors or a discrete observation model. 2. The model is fitted by sampling the posterior distribution of the model parameters. 3. Relevances of different covariates and interaction terms are computed and given as output. Covariate selection can be performed directly from the posterior distribution of the full model with all covariates included. The learned signal components can be visualized to study the magnitude and temporal aspects of different covariate effects. If a heterogeneous disease model was specified, the results inform about the heterogeneity of the possibly discovered disease effect. b) Illustration of different types of covariate effects that can be modeled using *lgpr*. The components $f^{(j)}$, $j = 1, \dots, 5$ are draws from Gaussian process priors. This artificial data comprises 8 individuals (4 male, 4 female), and 2 individuals of each sex are cases. The shown age-dependent components are a shared age effect $f^{(1)}$, a sex-specific deviation $f^{(2)}$ from the shared age effect, a disease-related age (*diseaseAge*) effect $f^{(3)}$, and a subject-specific deviation $f^{(5)}$ from the shared age effect. For each of the diseased individuals, the disease initiation occurs at a slightly different age, between 20 and 40 months. The component $f^{(4)}$ is a function of blood pressure only, but is plotted against age for consistency as the simulated blood pressure variable has a temporal trend. c) The cumulative effect $f = \sum_j f^{(j)}$ is a sum of the low-dimensional components. Our method learns each $f^{(j)}$ from data, without having to specify a parametric form.

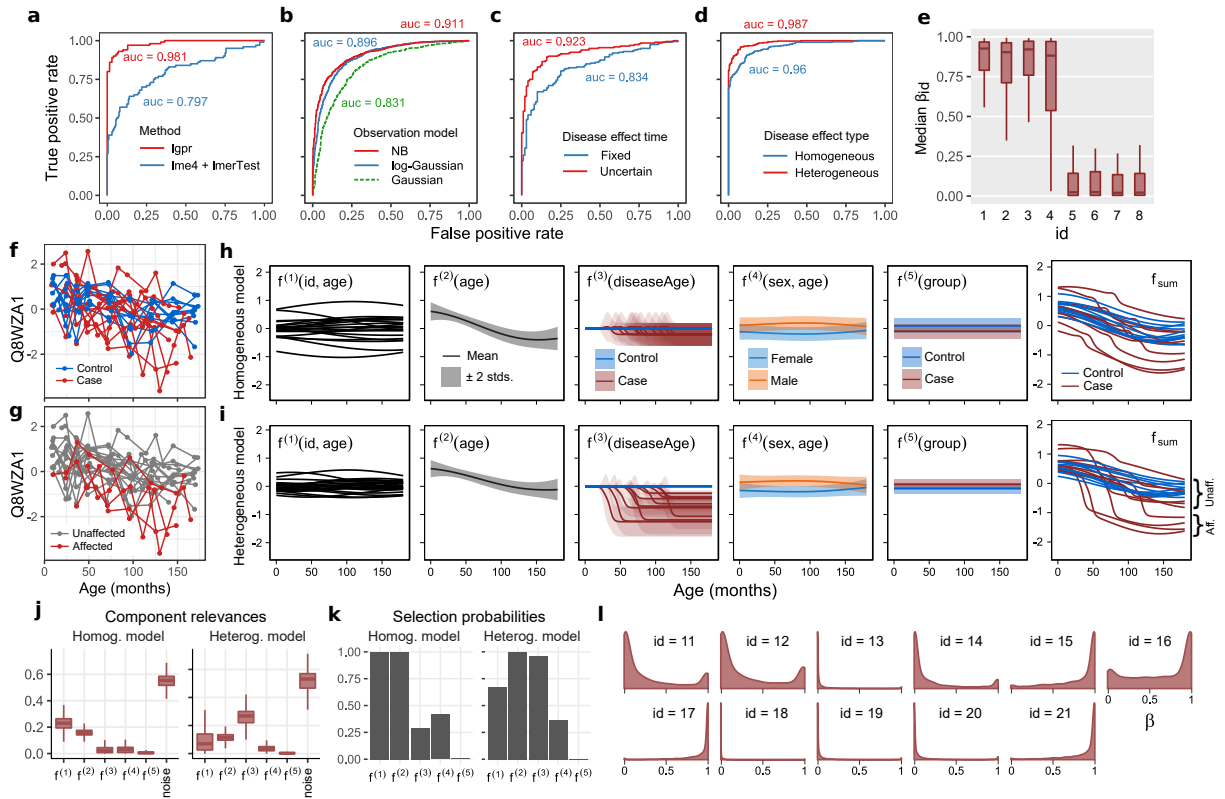


Figure 2 | Novel features of *lgpr* improve covariate selection accuracy and provide useful information about disease effects. **a-d)** Receiver operating characteristic (ROC) curves for the task of classifying covariates as relevant or irrelevant in simulated data experiments (described in Supplementary material). The ROC curves are computed over 100–300 simulated data sets each. **a)** Comparison between *lgpr* (our method) and linear mixed modeling using the *lme4* and *lmerTest* packages, when the true covariate effects are nonlinear. **b)** Using a discrete observation model improves covariate selection accuracy for negative binomially distributed count data. **c)** Modeling the uncertainty in disease effect time improves covariate selection accuracy, when the true effect has happened earlier than the clinically determined disease initiation. Here the ROC curve is for the task of classifying just the disease component as relevant or irrelevant (more details in Supplementary material, Figures S5-S6). **d)** Heterogeneous disease effect modeling improves covariate selection accuracy compared to the homogeneous approach, when the true disease effect is heterogeneous (4 out of 8 diseased individuals experience the effect). **e)** The individuals that experience the effect (id = 1–4) can be identified based on the posterior distribution of the β_{id} parameters, which are hyperparameters of our heterogeneous disease kernel, describing individual-specific disease effect magnitude. The boxplot describes the distribution of the posterior medians of the β_{id} parameters, over 100 simulated data sets (more details in Supplementary material, Figures S7-S8). The box is the interquartile range (*IQR*) between the 25th and 75th percentiles, vertical line inside the box is the 50th percentile, and the whiskers extend a distance of at most $1.5 \cdot IQR$ from the box boundary. **f) - i)** Results of analysing one example protein from a longitudinal proteomics data set. **f)** The normalized measurements for protein Q8WZA1, highlighted based on group (case or control). The lines connect an individual. **g)** Same data where four case individuals (id=15, 16, 17, 21) are highlighted, based on being determined as affected by the disease in heterogeneous modeling. **h)** Learned additive function components, as well as their sum f (using posterior mean parameters), for Q8WZA1 analyzed using the homogeneous and **i)** heterogeneous model. For clarity, standard deviations are not shown for $f^{(1)}$ and f_{sum} . **j)** Average relevances and **k)** selection probabilities for each component of the homogeneous and heterogeneous model. **l)** Kernel density estimates for the posterior distributions of the individual-specific disease effect magnitude parameters of the heterogeneous model.

An interpretable probabilistic machine learning method for heterogeneous longitudinal studies

Supplementary material

Juho Timonen, Henrik Mannerström, Aki Vehtari and Harri Lähdesmäki*
Department of Computer Science, Aalto University

October 31, 2021

arXiv:1912.03549v1 [stat.ML] 7 Dec 2019

Contents

1	Model	2
1.1	Gaussian processes	2
1.2	Additive GPs for longitudinal data	2
1.2.1	Continuous covariates	2
1.2.2	A zero-sum kernel for categorical covariates	3
1.2.3	Nonstationary disease effect modeling	3
1.3	Modeling a heterogeneous disease effect	4
1.4	Modeling uncertainty in the disease effect time	4
1.5	Observation models	5
2	Inference	5
2.1	Posterior inference	5
2.2	Covariate selection	6
2.3	Probabilistic covariate selection	8
2.4	Prior specification	8
3	Details of experiments with simulated data	8
3.1	Comparison with linear mixed effect modeling	9
3.2	Comparison with LonGP	9
3.3	Heterogeneous modeling of the disease effect	10
3.4	Modeling the uncertainty in disease effect time	11
3.5	Non-Gaussian data	11
4	Longitudinal proteomics data analysis	12
5	Related research	12
A	Proof of the zero-sum property	17
B	Figures S1-S8	18

*corresponding author

1 Model

1.1 Gaussian processes

A Gaussian process (GP) is a collection of random variables, any finite number of which has a multivariate normal distribution [1]. A function $f : \mathcal{X} \rightarrow \mathbb{R}$ has a GP prior $f(\mathbf{x}) \sim \mathcal{GP}(m(\mathbf{x}), k(\mathbf{x}, \mathbf{x}'))$ with mean function $m(\mathbf{x})$ and kernel function $k(\mathbf{x}, \mathbf{x}')$, if for any finite number of inputs $\{\mathbf{x}_p \in \mathcal{X}\}_{p=1}^P$, the vector of function values $\mathbf{f} = [f(\mathbf{x}_1), \dots, f(\mathbf{x}_P)]^\top$ has a multivariate normal prior $\mathbf{f} \sim \mathcal{N}(\mathbf{m}, \mathbf{K})$ with mean vector $\mathbf{m} = [m(\mathbf{x}_1), \dots, m(\mathbf{x}_P)]^\top$ and covariance matrix $\mathbf{K} \in \mathcal{X}^{P \times P}$ with entries $\{\mathbf{K}\}_{ij} = k(\mathbf{x}_i, \mathbf{x}_j)$. In this study, we only use a zero mean function $m(\mathbf{x}) = 0$. The kernel function must be positive semi-definite and it encodes information about the covariance of function values at different points. Choosing a suitable kernel function therefore is an essential part of GP modeling.

1.2 Additive GPs for longitudinal data

We denote a longitudinal data set with N data points, D covariates, and one response variable, by a tuple (\mathbf{X}, \mathbf{y}) , where \mathbf{X} is an $N \times D$ covariate matrix and $\mathbf{y} \in \mathbb{R}^N$ is a vector of measured responses. We refer to a row of \mathbf{X} by $\mathbf{x} \in \mathcal{X}$, where $\mathcal{X} = \times_{d=1}^D \mathcal{X}_d$ and \mathcal{X}_d is the set of possible values for covariate d . In general, \mathcal{X}_d can be a discrete set such as $\{\text{“Male”}, \text{“Female”}\}$ or a connected set such as \mathbb{R} . We assume that a time variable and a subject identifier variable are included in the set of available covariates, meaning that $D \geq 2$. It is possible that there is a different number of measurements for different subjects, and that the measurement times have irregular intervals. Since our focus is on biomedical data, we will from now on refer to subjects as individuals and measurement time as age.

In our modeling framework, we assume that there is an underlying unobserved signal $f : \mathcal{X} \rightarrow \mathbb{R}$ that is a function of the covariates. This signal is linked to the measured responses through a likelihood function, which is based on a statistical observation model. The process f is assumed to consist of J low-dimensional additive components, so that $f(\mathbf{x}) = f^{(1)}(\mathbf{x}) + \dots + f^{(J)}(\mathbf{x})$, where each $f^{(j)}$, $j = 1, \dots, J$ is a function of only one or two covariates. This is a sensible assumption in many real-world applications and apt to learn long-range structures in the data [2]. Furthermore, this decomposition into additive components allows us to obtain interpretable covariate effects after fitting the model. In our approach, each component has a GP prior $f^{(j)}(\mathbf{x}) \sim \mathcal{GP}(0, \alpha_j^2 k_j(\mathbf{x}, \mathbf{x}'))$, and because the components are *a priori* independent, we can write

$$f(\mathbf{x}) \sim \mathcal{GP}(0, k(\mathbf{x}, \mathbf{x}')), \quad (1)$$

where $k(\mathbf{x}, \mathbf{x}') = \sum_{j=1}^J \alpha_j^2 k_j(\mathbf{x}, \mathbf{x}')$. The parameter α_j^2 is called the marginal variance of component $f^{(j)}$ and it determines how largely the component varies. The base kernel functions $k_j(\mathbf{x}, \mathbf{x}')$ are constructed based on what covariates are included in the model and what modeling options are selected.

1.2.1 Continuous covariates

Shared effects of continuous covariates are modeled using the kernel

$$k_{\text{cont}}(\mathbf{x}, \mathbf{x}' | \ell_{\text{cont}}) = k_{\text{eq}}(x_{\text{cont}}, x'_{\text{cont}} | \ell_{\text{cont}}), \quad (2)$$

where

$$k_{\text{eq}}(x, x' | \ell) = \exp\left(-\frac{(x - x')^2}{2\ell^2}\right) \quad (3)$$

is the exponentiated quadratic kernel. Here, x_{cont} refers to a generic continuous covariate, each of which have their own lengthscale parameter ℓ_{cont} , which determines how rapidly the component can vary. For example, a shared age effect kernel is $k_{\text{age}}(\mathbf{x}, \mathbf{x}' | \ell_{\text{age}}) = k_{\text{eq}}(x_{\text{age}}, x'_{\text{age}} | \ell_{\text{age}})$.

1.2.2 A zero-sum kernel for categorical covariates

We assume that for any given individual, the value of a categorical covariate does not differ between time points. Effects of categorical covariates (such as id or sex) can be modeled either as time-dependent deviations from a shared age effect or as group-specific constant offsets. If x_{cat} is a categorical covariate with $M \geq 2$ categories, and whose effect is modeled in the time-dependent manner, the corresponding kernel function is

$$k_{\text{cat} \times \text{age}}(\mathbf{x}, \mathbf{x}' | \ell_{\text{cat}}) = k_{\text{zerosum}}(x_{\text{cat}}, x'_{\text{cat}}) \cdot k_{\text{eq}}(x_{\text{age}}, x'_{\text{age}} | \ell_{\text{cat}}), \quad (4)$$

where

$$k_{\text{zerosum}}(r, r') = \begin{cases} 1 & \text{if } r = r' \\ -\frac{1}{M-1} & \text{otherwise} \end{cases} \quad (5)$$

is the zero-sum kernel. This is similar to the Gaussian process ANOVA approach in [3]. It has a property that if $f : \mathbb{R} \times \{1, \dots, M\} \rightarrow \mathbb{R}$ is modeled as a GP $f \sim \mathcal{GP}(0, k_{\text{cat} \times \text{age}})$, the sum $\sum_{r=1}^M f(t, r)$ is always zero for any t (see proof in Appendix A). This means that f represents a time-dependent category-specific deviation from the shared age effect (see Figure S1 for illustration). In other words, the fact that the average across categories equals exactly zero for any t greatly helps model interpretation as this property guarantees that categorical covariates cannot bias the shared effects. Note that again x_{cat} refers to a generic categorical covariate, and each such covariate has its own lengthscale parameter ℓ_{cat} . This kernel structure can be used for modeling category-specific deviations from the shared effects of other continuous covariates as well, but it is left out of the focus of this study. In the time-independent case, the covariate effect corresponds to a constant offset for each category, and the corresponding kernel function is

$$k_{\text{offset}}(\mathbf{x}, \mathbf{x}') = k_{\text{zerosum}}(x_{\text{cat}}, x'_{\text{cat}}). \quad (6)$$

This is a special case of the time-dependent case when $\ell_{\text{cat}} \rightarrow \infty$, and can be used for example for modeling batch offsets that do not depend on time.

1.2.3 Nonstationary disease effect modeling

Disease effects are modeled using a nonstationary kernel for the disease-related age x_{disAge} , i.e. time from disease initiation or onset. This is motivated by the assumption that most changes in that function component occur near the event of disease occurrence, i.e. near $x_{\text{disAge}} = 0$. Note that for the control subjects, x_{disAge} is not observed at all. The disease kernel functions defined below actually will return 0 if either of the inputs corresponds to a healthy individual, but for cleaner notation, we write them assuming that there are no healthy individuals. Nonstationarity is achieved by first mapping the inputs through a monotonic nonlinear input warping function $\omega : \mathbb{R} \rightarrow]-1, 1[$, defined as

$$\omega(x | a) = 2 \cdot \left(\frac{1}{1 + e^{-ax}} - \frac{1}{2} \right), \quad (7)$$

where the parameter a controls the warping steepness, and then using the exponentiated quadratic kernel for the warped inputs. This approach was used in [4] where the kernel function was

$$k_{\text{ns}}(\mathbf{x}, \mathbf{x}' | a, \ell_{\text{disAge}}) = k_{\text{eq}}(\omega(x_{\text{disAge}} | a), \omega(x'_{\text{disAge}} | a) | \ell_{\text{disAge}}). \quad (8)$$

Whereas the kernel in Eq. 8 can model a nonstationary trend that is only present for the diseased individuals, its drawback is that it will also capture effects that are merely a different base level between the diseased and healthy individuals. For better interpretability, these effects should be explained by the binary covariate that describes membership of either of these two groups, instead of the continuous

disease-related age covariate. To account for this, we design a new kernel for the disease-related age component, defined as

$$k_{\text{disAge}}(\mathbf{x}, \mathbf{x}' | a, \ell_{\text{disAge}}) = f_{\text{vm}}(x_{\text{disAge}} | a) \cdot f_{\text{vm}}(x'_{\text{disAge}} | a) \cdot k_{\text{ns}}(\mathbf{x}, \mathbf{x}' | a, \ell_{\text{disAge}}), \quad (9)$$

where $f_{\text{vm}}(x | a) : \mathbb{R} \rightarrow]0, 1[$ is a variance mask function that forces the disease component to have zero variance, i.e. the same value for both groups, when $x \rightarrow -\infty$. We choose to use

$$f_{\text{vm}}(x | a) = \frac{1}{1 + e^{-a(x-r)}}, \quad (10)$$

which means that the allowed amount of variance between these groups rises sigmoidally from 0 to the level determined by the marginal variance parameter, so that the midpoint is at $r = \frac{1}{a} \log\left(\frac{h}{1-h}\right)$ and $\omega(r | a) = 2h - 1$. The parameter h therefore determines a connection between the regions where the disease component is allowed to vary between the two groups and where it is allowed to vary over time. In our experiments, we use the value $h = 0.025$. This means, that 95% of the variation in ω occurs on the interval $[-r, r]$. The disease kernels in Eq. 8 and Eq. 9 as well as functions drawn from the corresponding GP priors are demonstrated in Figure S4.

1.3 Modeling a heterogeneous disease effect

In Eq. 9, we presented a kernel for modeling a disease effect that is equally strong for all diagnosed individuals. In order to allow effects whose strength is heterogeneous over the diagnosed individuals or is completely absent from some case individuals, we define additional parameters $\boldsymbol{\beta} = [\beta_1, \dots, \beta_Q]$, where Q is the number of diagnosed individuals and each $\beta_i \in [0, 1]$. We design a new kernel

$$k_{\text{heter}}(\mathbf{x}, \mathbf{x}' | a, \ell_{\text{disAge}}, \boldsymbol{\beta}) = \sqrt{\beta_q \beta_{q'}} \cdot k_{\text{disAge}}(\mathbf{x}, \mathbf{x}' | a, \ell_{\text{disAge}}), \quad (11)$$

where the case indices $q = \mathcal{I}(x_{id})$ and $q' = \mathcal{I}(x'_{id})$ are determined by a bijection $\mathcal{I} : \mathcal{X}_{\text{caseID}} \rightarrow \{1, \dots, Q\}$, where $\mathcal{X}_{\text{caseID}}$ is the set of subject IDs for the case individuals. In other words, we want to allow effects of different magnitude for different case subjects, yet using all available statistical power by modeling the effects of diseased individuals as correlated. In our implementation, the prior for the unknown parameters $\boldsymbol{\beta}$ is set to $\beta_i \sim \text{Beta}(b_1, b_2)$, where the shape parameters b_1 and b_2 can be defined by the user. By default, we set $b_1 = b_2 = 0.2$, in which case most of the prior mass is near the extremes 0 and 1 (Figure S2c). The posterior distributions of β_i can then be used to make inferences about which case individuals are affected by the disease. The kernel in Eq. 11 is illustrated in Figure 4, along with functions drawn from the corresponding GP prior.

1.4 Modeling uncertainty in the disease effect time

The presented disease effect modeling approach relies on observing the disease-related age for each case individual. It is defined as $x_{\text{disAge}} = x_{\text{age}} - t'_q$ for diseased individual q , where t'_q is the disease effect time for that subject. In [4], this effect time was defined as the age of subject q at the clinically determined disease initiation time, but in general the effect time can differ from it. Our implementation allows Bayesian inference also for the effect times, and can therefore capture nonstationary disease effects that for some or all individuals occur at a different time point than the clinically determined initiation. The user can set the prior either directly for the effect time t' , or for the difference between the effect time and observed initiation time, $\Delta t = t^{\text{obs}} - t'$. The first option is suitable if the disease is known to commence at certain age for all individuals. The latter option is useful in a more realistic setting where such information is not available, and one would like to set the prior so that the clinically determined initiation times t^{obs} have a high probability.

1.5 Observation models

We have implemented five different likelihood models that relate the observed data and the underlying signal f . Below, we use notation $f_i = f(\mathbf{x}_i)$, $\bar{y} = \frac{1}{N} \sum_{i=1}^N y_i$, $\text{logistic}(x) = \frac{1}{1+\exp(-x)}$ and $\text{logit}(x) = \log\left(\frac{x}{1-x}\right)$.

- The Gaussian observation model for continuous data is $y_i = f_i + \varepsilon_i$, where $\varepsilon_i \sim \mathcal{N}(0, \sigma_e^2)$. The parameter σ_e^2 which quantifies noise variance.
- The Bernoulli observation model for binary data is $y_i \sim \text{Bernoulli}(p_i)$, where $p_i = \text{logistic}(\hat{C} + f_i)$ is the success probability. By default, we set $\hat{C} = \text{logit}(\bar{y})$.
- In the binomial observation model for count data, the vector containing the numbers of trials $\boldsymbol{\eta} = [\eta_1, \dots, \eta_N]^\top$ is supplied as data, along with \mathbf{y} , which now is the vector of numbers of observed successes. The model is $y_i \sim \text{Binomial}(p_i, \eta_i)$, where $p_i = \text{logistic}(\hat{C} + f_i)$ is the success probability. By default, we set $\hat{C} = \text{logit}\left(\frac{1}{N} \sum_{i=1}^N y_i / \eta_i\right)$.
- The Poisson observation model for count data is $y_i \sim \text{Poisson}\left(\exp(\hat{C} + f_i)\right)$. By default, we set $\hat{C} = \log(\bar{y})$.
- The negative binomial (NB) observation model for count data is $y_i \sim \text{NB}\left(\exp(\hat{C} + f_i), \phi\right)$, where ϕ is an inverse overdispersion parameter. By default, we set $\hat{C} = \log(\bar{y})$. Here we use the parametrization for which

$$X \sim \text{NegBinomial}(x, \phi) \quad \iff \quad \text{E}[X] = x, \quad \text{Var}[X] = x + \frac{x^2}{\phi}. \quad (12)$$

Our software package, *lgpr*, can be easily extended with additional observation models depending on users' needs.

2 Inference

2.1 Posterior inference

Our covariate selection procedure relies on first building a full model which includes all available covariates, and then studying the posterior distribution of the unknowns of this model, mostly focusing on that of the function components. We collect all marginal variances, lengthscales and other possible kernel hyperparameters into a vector $\boldsymbol{\theta}_{\text{kernel}}$. Similarly, we denote the parameters related to the observation model by $\boldsymbol{\theta}_{\text{obs}}$ and other parameters such as those related to input uncertainty by $\boldsymbol{\theta}_{\text{other}}$. The collection of all unknown model parameters is then $\boldsymbol{\theta} = \{\boldsymbol{\theta}_{\text{kernel}}, \boldsymbol{\theta}_{\text{obs}}, \boldsymbol{\theta}_{\text{other}}\}$. We use the dynamic Hamiltonian Monte Carlo sampler [5] with multinomial sampling of dynamic length trajectories [6], as implemented in Stan [7], to draw S samples from the posterior distribution of $\boldsymbol{\theta}$.

The remaining unknowns of the model are the values of the function components, for which we use the notation $\mathbf{f}^{(j)} = [f^{(j)}(\mathbf{x}_1), \dots, f^{(j)}(\mathbf{x}_N)]^\top$, where \mathbf{x}_i is the i th row of \mathbf{X} , and $\mathbf{f} = \sum_{j=1}^J \mathbf{f}^{(j)}$. Under the Gaussian observation model and fixed parameters $\boldsymbol{\theta}$, the posterior distributions of $\mathbf{f}^{(1)}, \dots, \mathbf{f}^{(J)}$ and \mathbf{f} can be derived analytically. For readability, we for now assume that $\boldsymbol{\theta}$ are fixed and drop the dependency on $\boldsymbol{\theta}_{\text{kernel}}$ off the notation of kernel matrices. The kernel matrix corresponding to component j is denoted by $\mathbf{K}^{(j)}$, and its entries are $\{\mathbf{K}^{(j)}\}_{ik} = \alpha_j^2 k_j(\mathbf{x}_i, \mathbf{x}_k \mid \boldsymbol{\theta}_{\text{kernel}})$, and the full additive kernel matrix is denoted by $\mathbf{K} = \sum_{j=1}^J \mathbf{K}^{(j)}$. Under the Gaussian observation model and the prior of \mathbf{f} defined by Eq. 1, the joint density of \mathbf{y} and \mathbf{f} is also Gaussian

$$\begin{bmatrix} \mathbf{f} \\ \mathbf{y} \end{bmatrix} \sim \mathcal{N}\left(\begin{bmatrix} \mathbf{0} \\ \mathbf{f} \end{bmatrix}, \begin{bmatrix} \mathbf{K} & \mathbf{K} \\ \mathbf{K} & \mathbf{K} + \sigma_e^2 \mathbf{I} \end{bmatrix}\right). \quad (13)$$

Using the Gaussian conditioning formula, we get the posterior $p(\mathbf{f} | \mathbf{y}) = \mathcal{N}(\mathbf{f} | \boldsymbol{\mu}, \boldsymbol{\Sigma})$, where

$$\begin{cases} \boldsymbol{\mu} &= \mathbf{K}(\mathbf{K} + \sigma_e^2 \mathbf{I})^{-1} \mathbf{y} \\ \boldsymbol{\Sigma} &= \mathbf{K} - \mathbf{K}(\mathbf{K} + \sigma_e^2 \mathbf{I})^{-1} \mathbf{K} \end{cases} \quad (14)$$

Similarly, the posterior distribution of component j becomes $p(\mathbf{f}^{(j)} | \mathbf{y}) = \mathcal{N}(\mathbf{f}^{(j)} | \boldsymbol{\mu}^{(j)}, \boldsymbol{\Sigma}^{(j)})$, where

$$\begin{cases} \boldsymbol{\mu}^{(j)} &= \mathbf{K}^{(j)}(\mathbf{K} + \sigma_e^2 \mathbf{I})^{-1} \mathbf{y} \\ \boldsymbol{\Sigma}^{(j)} &= \mathbf{K}^{(j)} - \mathbf{K}^{(j)}(\mathbf{K} + \sigma_e^2 \mathbf{I})^{-1} \mathbf{K}^{(j)} \end{cases} \quad (15)$$

Furthermore, the posterior distribution of $\mathbf{f}^* = [f(\mathbf{x}_1^*), \dots, f(\mathbf{x}_P^*)]^\top$, where \mathbf{x}_p^* , $p = 1, \dots, P$ are unobserved data points is $p(\mathbf{f}^* | \mathbf{y}) = \mathcal{N}(\boldsymbol{\mu}^*, \boldsymbol{\Sigma}^*)$ with

$$\begin{cases} \boldsymbol{\mu}^* &= \mathbf{K}_*(\mathbf{K} + \sigma_e^2 \mathbf{I})^{-1} \mathbf{y} \\ \boldsymbol{\Sigma}^* &= \mathbf{K}_{**} - \mathbf{K}_*(\mathbf{K} + \sigma_e^2 \mathbf{I})^{-1} \mathbf{K}_*^\top \end{cases} \quad (16)$$

where \mathbf{K}_* is the $P \times N$ kernel matrix between test and data points, and \mathbf{K}_{**} is the $P \times P$ kernel matrix between test points. We then obtain the posterior predictive distribution

$$p(\mathbf{y}^* | \mathbf{y}) = \mathcal{N}(\boldsymbol{\mu}^*, \boldsymbol{\Sigma}^* + \sigma^2 \mathbf{I}). \quad (17)$$

Also the component posteriors $p(\mathbf{f}_*^{(j)} | \mathbf{y})$ are multivariate Gaussian with mean and covariance

$$\begin{cases} \boldsymbol{\mu}_*^{(j)} &= \mathbf{K}_*^{(j)}(\mathbf{K} + \sigma_e^2 \mathbf{I})^{-1} \mathbf{y} \\ \boldsymbol{\Sigma}_*^{(j)} &= \mathbf{K}_{**}^{(j)} - \mathbf{K}_*^{(j)}(\mathbf{K} + \sigma_e^2 \mathbf{I})^{-1} \mathbf{K}_*^{(j)\top} \end{cases} \quad (18)$$

where the kernel matrices with superscript j are computed using only the j th kernel function. Eqs. 17 and 18 are needed in this study only for visualization purposes. For the non-Gaussian observation models, the posterior distributions of \mathbf{f} or $\mathbf{f}^{(j)}$ given fixed hyperparameters are not available analytically. In this case we therefore sample the posterior of each $\mathbf{f}^{(j)}$ simultaneously with $\boldsymbol{\theta}$. Because these function values will have strong posterior correlations, we reparametrize the problem using Cholesky decompositions of the kernel matrices $\mathbf{K}^{(j)} = \mathbf{L}^{(j)} \mathbf{L}^{(j)\top}$, so that we only need to sample auxiliary variables $\boldsymbol{\xi}^{(j)}$, which are defined by $\mathbf{f}^{(j)} = \mathbf{L}^{(j)} \boldsymbol{\xi}^{(j)}$ and have less posterior correlations.

2.2 Covariate selection

In our covariate selection method, we first determine the proportion of variance explained by noise and each function component. After posterior sampling, we have S parameter samples $\{\boldsymbol{\theta}^{(s)}\}_{s=1}^S$ and in the case of a non-Gaussian observation model, also samples $\{\mathbf{f}^{(j,s)}\}_{s=1}^S$ of each function component $j = 1, \dots, J$. For each sample s , our model gives predictions $\mathbf{y}_s^* = [y_{1,s}^*, \dots, y_{N,s}^*]$. These are defined differently depending on the observation model.

- When using the Gaussian observation model, these are defined as $\mathbf{y}_s^* = \boldsymbol{\mu}_s$, i.e. the analytically computed mean prediction in Eq. 14 with parameter values set to $\boldsymbol{\theta}^{(s)}$.
- With Poisson or NB model we use $\mathbf{y}_s^* = \exp\left(\hat{C} + \sum_{j=1}^J \mathbf{f}^{(j,s)}\right)$.
- With Bernoulli model $\mathbf{y}_s^* = \text{logistic}\left(\hat{C} + \sum_{j=1}^J \mathbf{f}^{(j,s)}\right)$.
- With Binomial model, $\mathbf{y}_s^* = \boldsymbol{\eta} \odot \text{logistic}\left(\hat{C} + \sum_{j=1}^J \mathbf{f}^{(j,s)}\right)^*$.

* \odot = elementwise multiplication

The constant \hat{C} is defined for each model as in Section 1.5. To determine how much of the data is explained by noise, we compute

$$p_{\text{noise}}^{(s)} = \frac{RSS_s}{ESS_s + RSS_s} \in [0, 1] \quad (19)$$

using the residual sum of squares $RSS_s = \sum_{i=1}^N (y_{i,s}^* - y_i)^2$ and explained sum of squares $ESS_s = \sum_{i=1}^N (y_{i,s}^* - \bar{y}_s^*)^2$, where $\bar{y}_s^* = \frac{1}{N} \sum_{i=1}^N y_{i,s}^*$. Note that in ordinary linear regression, one would typically use $\bar{y} = \frac{1}{N} \sum_{i=1}^N y_i$ in the place of \bar{y}_s^* so that $ESS + RSS = TSS = \sum_{i=1}^N (y_i - \bar{y})^2$. However, for general nonlinear regression, this decomposition does not hold. Furthermore, the related classical R^2 statistic is problematic for Bayesian models [8]. We argue that for our model it is more reasonable to define ESS based on the variation of the predictions instead of based on the squared difference of predictions and the mean of observed data. With our definition, $p_{\text{noise}}^{(s)}$ will be one if the model gives constant predictions and zero if predictions match data exactly.

After computing $p_{\text{noise}}^{(s)}$, we further divide the proportion of variance that is associated with the actual signal, $p_{\text{signal}}^{(s)} = 1 - p_{\text{noise}}^{(s)}$, for each model component. For cleaner notation, we define the variation of a vector $\mathbf{v} = [v_1, \dots, v_L]$ as a sum of squared differences from the mean, i.e. $SS(\mathbf{v}) = \sum_{l=1}^L (v_l - \bar{v}_l)^2$. The relevance of component j , in sample s , is defined as

$$\text{rel}_j^{(s)} = \left(1 - p_{\text{noise}}^{(s)}\right) \frac{SS_j^{(s)}}{\sum_{j'=1}^J SS_{j'}^{(s)}} \quad (20)$$

where $SS_j^{(s)} = SS(\boldsymbol{\mu}^{(j,s)})$ with Gaussian observation model and $SS_j^{(s)} = SS(\mathbf{f}^{(j,s)})$ otherwise. Above we used $\boldsymbol{\mu}^{(j,s)}$ to denote the mean vector in Eq. 15, corresponding to sample s . The final component and noise relevances are then obtained as averages

$$\text{rel}_j = \frac{1}{S} \sum_{s=1}^S \text{rel}_j^{(s)} \quad \text{and} \quad p_{\text{noise}} = \frac{1}{S} \sum_{s=1}^S p_{\text{noise}}^{(s)} \quad (21)$$

over the S MCMC samples. Our definition of component relevances has the beneficial property that we can compute the proportion of variance explained by a subset of components $\mathcal{J} \subseteq \{1, \dots, J\}$ simply as

$$\text{rel}_{\mathcal{J}} = \sum_{j \in \mathcal{J}} \text{rel}_j. \quad (22)$$

Furthermore, it follows that

1. $\text{rel}_{\{1, \dots, J\}} = 1 - p_{\text{noise}} = p_{\text{signal}}$
2. $\text{rel}_A < \text{rel}_B$ if $A, B \subseteq \{1, \dots, J\}$ and $A \subset B$
3. $\text{rel}_{\emptyset} = 0$.

Property 2 states that adding more components will always increase the explained variance. Therefore, our covariate selection method is based on selecting the minimal subset of components \mathcal{J}_{sel} that together with noise explain at least $T\%$ of variance. Formally,

$$\mathcal{J}_{\text{sel}} = \arg \min_{\mathcal{J}} |\mathcal{J}| \quad \text{s.t.} \quad \text{rel}_{\mathcal{J}} + p_{\text{noise}} \geq \frac{T}{100}, \quad (23)$$

and $T = 95$ by default. The user change the desired threshold T according their preferences, taking into account the total number of model components and amount of noise in the data. In the sense of selecting a minimal subset of covariates based on inference of a full model with all covariates, our

method is similar to the projection predictive model selection method [9], which has been shown to perform well in predictive covariate selection for generalized linear models [10]. However, in our case finding the minimal subset is trivial and does not require additional sampling or parameter fitting. Due to the additivity property in Eq. 22, it reduces to just sorting the list of relevances $\{\text{rel}_1, \dots, \text{rel}_J\}$. Furthermore, computing relevances based on only the full model with all covariates included provides a safeguard against overfitting during a sequential subset search. This is exceptionally important because our model usually contains components that have different complexities. For example, an individual-specific age component has the ability to model more complex data than a group-specific age component.

The selected covariates and interactions are defined directly as the variables that the selected components are functions of.

2.3 Probabilistic covariate selection

The above selection strategy is to tackle the task of classifying a component/covariate as relevant or irrelevant. To provide a more informative and interpretable results, we present here a method for computing a selection probability for each component. The method is based on defining the relevance of component j in sample s as in Equation 20 and repeating the selection procedure in Eq. 23 for each sample $s = 1, \dots, S$ separately. The selection probability $p_j(T)$ of component j is then the proportion of times it was selected in the total S selection tasks. This method still requires setting the threshold T , but is less sensitive with respect to it than the non-probabilistic selection. In order to avoid having to set a fixed threshold T at all, one can instead compute the selection probabilities as

$$p_j = \int_0^1 p_j(T)w(T)dT, \quad (24)$$

where $w(T)$ is a weight distribution that satisfies $\int_0^1 w(T)dT = 1$. Our package provides a routine for this using simple numerical quadrature.

2.4 Prior specification

Our software implementation allows the user to set various different priors for the sampled hyperparameters. To allow general prior specifications for the lengthscales, all continuous covariates are scaled to have unit variance and zero mean. An exception to this is the disease-related age, because its lengthscale prior needs to be set only for the warped inputs that lie on the interval $[-1, 1]$. When using the Gaussian observation model, also the response variable is standardized this way for easier specification of priors for the marginal variance and noise variance parameters. Unless otherwise stated in the experiments, we use a Student- t_ν^+ prior with $\nu = 20$ for all marginal standard deviations, and a Log-Normal(0, 1) prior for the lengthscale parameters. If using the Gaussian observation model, we use an Inverse-Gamma(2, 1) prior for the noise variance parameter. For the input warping steepness, our default prior is Inverse-Gamma(14, 5), which has most of its probability mass between 0.2 and 0.8. These are set based on assuming that the disease-related age is expressed in months. At extreme case $a = 0.2$, the input warping (Eq. 7) allows changes in the disease component virtually only 24 months before and after the disease effect time point. At the other end, the value $a = 0.8$ allows the disease component to vary virtually only 6 months before and after the effect time point. The default priors are visualized in Figure S2.

3 Details of experiments with simulated data

We use simulated data to create various scenarios for testing the presented modeling and covariate selection framework. In each experiment, we generate artificial longitudinal data sets that comprise several individuals and multiple measurements for each individual. The number of measurement points

P is the same for each individual. In addition to having subject id and age as covariates, we also generate different types of continuous and categorical covariates. For each individual the value of any categorical group covariate is constant over all time points and is drawn from the binomial distribution with $p = 0.5$. Continuous covariates other than age and disease-related age are generated so that for each subject i , the value of covariate x at the k th measurement point is $x_{ik} = \sin(a_i \cdot s_k + b_i) + c_i$, where s_1, \dots, s_P are equispaced on the interval $[0, 2\pi]$ and the values a_i, b_i, c_i are drawn independently for each subject and covariate so that $a_i \sim \text{Uniform}[\frac{\pi}{8}, \frac{\pi}{4}]$, $b_i \sim \text{Uniform}[\pi, 2\pi]$ and $c_i \sim \text{Uniform}[-0.5, 0.5]$. In order to test how accurately the relevant covariates can be identified, we simulate the response variable so that some covariates are relevant and some are not. To be specific, we first generate additive components \mathbf{f}_j from GP priors, as illustrated in Main Figure 1. The components are scaled so that the effect size (variance) is one for relevant components and zero for the irrelevant ones. Effects of categorical covariates are always included as deviations from a shared age effect in both simulation and inference. The response variable measurements \mathbf{y} are generated from \mathbf{f} by adding Gaussian distributed noise, except for in our experiment with count data (Section 3.5). In the experiments, we run four independent dynamic HMC chains for 2000 iterations, and the first half of each chain is considered as warmup. In each experiment we generate several random replications of the simulation and measure performance in classifying covariates into relevant or irrelevant using the area under curve (AUC) measure for receiver operating characteristic (ROC) curves. Higher AUC value indicates better performance. The computed covariate relevances (Eq. 21) are used as a score in the ROC analysis, which is performed using the *pROC* package [11].

3.1 Comparison with linear mixed effect modeling

In the first experiment we confirm that the linear mixed modeling approach cannot capture the covariate relevances whereas our GP modeling approach can, when the covariate effects are nonlinear. In order to demonstrate that our method also scales to larger data sets, we repeat the comparison using $N = 100, 300$ and 600 as the data set size, generating 100 data sets in each case. We set the signal-to-noise ratio to only 0.2 so that a lot of data is required to reveal the relevant covariates. The 100, 300 and 600 data points are generated so that the number of individuals is 20, 30, and 30, and the measurement times are at $\{12 \cdot m\}_{m=1}^5$, $\{6 \cdot i\}_{m=1}^{10}$ and $\{3 \cdot m\}_{m=1}^{20}$ months, respectively. We generate data so that it contains an individual-specific and a shared age effect, as well as three categorical covariates z_1, z_2, z_3 out of which only z_1 is relevant. A lengthscale of 24 months is used to draw the shared age component, and a lengthscale of 12 months for the individual and category-specific age-dependent deviation components. In linear mixed effect modeling, we use the `lmer` model fitting command of the *lme4* package [12] with formula $\mathbf{y} \sim 1 + \text{age} + (\text{age}|\text{id}) + \mathbf{z1} + \mathbf{z2} + \mathbf{z3}$. Significance of the covariates $z_j, j = 1, 2, 3$ is then estimated with the *lmerTest* package [13] by computing the p -value of an F-test for single-term deletions with the default Satterthwaite approximation for denominator degrees of freedom. Because it is not straightforward to compute covariate significances for the id and age covariates in linear mixed effect modeling, we restrict the covariate selection problem to only these three categorical covariates. In GP modeling, the covariate relevances are inferred by sampling the full model with an individual-specific and a shared age component, as well as one category-specific deviation component corresponding to each categorical covariate. We generate 100 data sets independently, and compute ROC curves using the p -values as a score in linear modeling. The resulting ROC curves and AUC scores are shown in Figure S3a.

3.2 Comparison with LonGP

We also compare our method with the additive Gaussian process model selection method *LonGP* [4], which models non-stationary disease effects using the kernel in Eq. 8. Here we set up a more difficult covariate selection problem with more covariates of different types. We generate individual-specific,

shared, and disease-related age effects, as well as four other categorical covariates that interact with age as category-specific age-dependent deviations from the shared age effect, and four more continuous covariates. We generate data with 16 individuals, measured at time points 12, 24, 36, 48, 60 and 72 months, resulting in $N = 96$ data points. Furthermore, we add Gaussian jitter with $\sigma_t = 1$ to the measurement times to make the data unequally spaced and more realistic. The individual-specific, shared, and two of the categorical covariates’ age effects are set to be relevant with lengthscale 24 months for shared and 12 months for other age effect components. Also two of the additional continuous covariates are set as relevant with lengthscale 1. Two of the continuous and two of the categorical covariates are left as irrelevant. Furthermore, half of the individuals are considered diseased and a disease effect time is drawn for each of them separately, uniformly from the interval [36, 48] months. This time point is used to simulate a nonstationary disease effect, using the kernel in Eq. 9, with the steepness a drawn randomly from $\mathcal{N}(0.5, 0.1^2)$. However, during inference, we fix the effect time to the next actual measurement time. We first generate 100 data sets where also a disease-related age effect is relevant, with lengthscale 1, and then another 100 data sets with no disease effect. Gaussian noise is added so that signal-to-noise ratio is 3.

LonGP uses a greedy forward search where at each step, the component that has the best leave-one-out cross-validation or stratified cross-validation score is added to the model if the score exceeds a pre-specified threshold. We use the default thresholds LOOCVR = 0.8 and SCVR = 0.95. By default, the id covariate has to be in the model for *LonGP* and the continuous covariates are searched first before the categorical ones. When categorical covariates are added, also their interaction component with age is added if age is already in the model. If the shared age component is not in the model, the categorical covariates act only as group offsets. In order to create a comparable scenario with this complicated procedure, we use *LonGP* so that also the shared age component is by default in the model, and leave the id and age covariates out of the selection problem, while their effect is still modeled. The covariates that are supposed to be classified as either relevant or irrelevant are therefore categorical covariates z_i , $i = 1, \dots, 4$, continuous covariates x_i , $i = 1, \dots, 4$ and the disease-related age. The hyperparameter priors are same for both models. However, the input warping steepness cannot be inferred in *LonGP*, so we use its default fixed value $a = 0.5$. We use a categorical kernel (returns 1 if categories are same, 0 otherwise) for terms that contain a categorical covariate, because *LonGP* can not model zero-sum deviations.

Since *LonGP* uses a sequential model search, we cannot compute full ROC curves for it. Therefore we compare performances by counting how often each covariate is selected. Figure S3b shows the number of times each method selected different covariates across the 100 simulated data sets for both the case where the disease effect was and was not relevant. *LonGP* tends to select very few covariates, and to have comparable results for *lgpr*, we set a rather low threshold of $T = 80$ in Eq. 23. We see that *lgpr* can more clearly distinguish the relevant covariates from the irrelevant covariates. In this simulation scenario, the total covariate selection accuracy for *lgpr* is 81.4% when the disease-related age is relevant and 87.0% when it is not. Corresponding numbers for *lonGP* are 65.0% and 75.2%. Furthermore, the average run time per data set is approximately five times longer for *LonGP* (Figure S3b).

3.3 Heterogeneous modeling of the disease effect

To test the heterogeneous disease effect modeling approach, we generate data with 16 individuals out of which 8 are diagnosed with the disease but so that the disease effect is generated for only $N_{\text{affected}} = 0, 2, 4, 6$ or 8 of them. The measurement points in this experiment are exactly 12, 24, 36, 48, 60 and 72 months, and the disease effect time for each diagnosed individual is sampled uniformly from the interval [46, 48] months, but it is observed at 48 months. In addition to the disease component, we also create relevant individual-specific and shared age effects, and one relevant (z_1) and two irrelevant (z_2, z_3) categorical covariates that interact with age. The used lengthscales are 24 months for shared age, 1 for the disease component and 18 months for other components. All covariates are considered to be subject to selection. We set the signal-to-noise ratio to 3 and simulate a total of 500 data sets,

100 for each case $N_{\text{affected}} = 0, 2, 4, 6, 8$. In the case $N_{\text{affected}} = 8$ all diseased individuals have the effect and for $N_{\text{affected}} = 0$ none do, meaning that the disease-related age is an irrelevant covariate. For each data set replication, the inference is done using both a heterogeneous and homogeneous model. The results in Figure S7 show that heterogeneous modeling improves covariate selection accuracy, and the improvement is clearest when only 2 of the individuals actually have the effect. In heterogeneous modeling, the samples of the individual-specific disease effect magnitude parameters β_{id} indicate the affected individuals. See Figure S8 for a demonstration of heterogeneous model inference.

3.4 Modeling the uncertainty in disease effect time

To test the model where the disease effect time is considered to be uncertain, we simulated data where the observed disease initiation time is later than the true generated effect of the disease-related age covariate. In this experiment we have 12 individuals, 6 of them diseased, measured at 12, 24, 36, 48, 60, 72, 84 and 96 months and we use a signal-to-noise ratio 1. The components and covariates, as well as the lengthscales are same as in the previous experiment. For each diseased individual q , the real effect age t'_q is sampled from the normal distribution with mean 36 and standard deviation 4 months Figure S5a. The disease is considered observable at age $\tau_q = \min\{t'_q + t_q^*, 96\}$ months, where t_q^* is drawn from the exponential distribution with rate parameter 0.05 (Figure S5b). The disease onset is then observed to be at the next measurement time point

$$t_q^{\text{obs}} = \arg \min_t t \quad \text{s.t.} \quad t \geq \tau_q, \quad t \in \{12, 24, 36, 48, 60, 72, 84, 96\} \quad (25)$$

and the observed disease ages are computed as $x_{\text{disAge}} = x_{\text{age}} - t_q^{\text{obs}}$. We simulate 300 data sets so that the relevant covariates are

- id, age and z_1 in the first 100
- age, diseaseAge and z_1 in the next 100
- id, age, diseaseAge and z_1 in the last 100

data sets. For each data set we run the inference first by fixing the effect time to equal the clinically determined onset time, and then using two different priors for the effect time uncertainty. The first prior is $\Delta t \sim \text{Exp}(0.05)$, meaning that the observed onset is most likely, and prior mass decays exponentially towards birth. An oracle prior, which is exactly the distribution that is used to sample the real effect time, is used for reference. The results in Figure S5c show that the uncertainty modeling improves the covariate selection accuracy, and the oracle prior performs best as expected. Especially, we see that detection of the disease-related age covariate is more accurate when the uncertainty is being modeled Figure S5d. See Figure S6a for a demonstration of effect time inference.

3.5 Non-Gaussian data

To demonstrate the benefit of using a proper observation model, we generate negative binomially distributed count data and model it using different observation models. We generate measurements for 10 individuals at timepoints 6, 12, 18, 24, 30, 36, 42 and 48 months with jitter $\sigma_t = 0.2$ months. The data contains the covariates id and age and additionally two categorical covariates z_1, z_2 and two continuous covariates x_1, x_2 . We use lengthscale 12 months to simulate the shared age component and 6 months for the group and individual specific age effects. We simulate 300 data sets so that the relevant covariates are

- age , x_1 and z_1 in the first 100
- id, age, x_1 , and z_1 in the next 100

- just x_1 and x_2 in the last 100

data sets. The process \mathbf{f} is generated from the additive Gaussian process prior and scaled to have variance 2. The measurements are drawn from $\mathbf{y} \sim \text{NB}(\exp(-1 + \mathbf{f}), \phi)$ with $\phi = 2$. This will create integer-valued data with many zeros. For each data set, we run the inference using a Gaussian and negative binomial observation model, with 4 MCMC chains and 4000 iterations each chain. The latter involves the sampled parameter ϕ , for which we use a Log-Normal(1, 1) prior. Results in Main Figure 2d confirm that the covariate selection for this kind of negative binomial distributed count data cannot be done reliably using the Gaussian observation model, whereas using the correct observation model in *lgpr* model improves the covariate selection accuracy. For reference, we also run the inference using Gaussian observation model but so that the data is first transformed through the mapping $y \mapsto \log(1 + y)$. We note, however, that covariate selection performance of the Gaussian model improves (relative to that of negative binomial model) when data has higher count values and dispersion is smaller, i.e., when negative binomial model is approximated well by the Gaussian model.

4 Longitudinal proteomics data analysis

Protein intensities were measured from plasma samples of 21 children, with nine measurement time points for each child, resulting in a total of 189 data points for most proteins. We chose to analyze 1538 proteins which were chosen by requiring that at least 50% of the measurements must have non-missing values. The exact sample sizes after discarding missing data for each protein are shown in Table S1. 11 of the children developed Type 1 diabetes (T1D), and for those individuals we defined the disease effect time to be the seroconversion age, which was defined as age at the first detection of one or multiple T1D autoantibodies [14]. Like in [4], we performed our modeling using five covariates: id, age, diseaseAge, sex and group (case/control). Each protein was analyzed separately, and we followed the preprocessing described in [14] to get normalized protein intensities. Of the categorical covariates, id and sex are modeled as age-dependent category-specific deviations from the shared age effect, and group is a constant group offset variable. For diseaseAge, the variance mask kernel in Eq. 9 is used. We used the Gaussian observation model after normalizing the protein intensities. We performed the analysis for all proteins using both the the homogeneous and the heterogeneous disease effect modeling approach (Eq. 11), in which case the prior for the additional β parameters is Beta(0.2, 0.2). We run four independent MCMC chains, using 4000 iterations for each protein, discarding the first half of each chain as warmup. For a handful of proteins the mixing of chains was slower (\hat{R} -statistic [15] > 1.05 with initial number of iterations), and we rerun the sampling doubling the number of iterations. We used the 95% threshold (in Eq. 23) for covariate selection. In order to avoid fitting to artifacts in the data, we interpreted the heterogeneous modeling results so that the disease-related age covariate was selected only if it was found for at least three case individuals (median of the individual-specific disease effect magnitude parameter > 0.5).

5 Related research

Frequentist modeling of longitudinal data has a long history [16, 17]. Random-effect models, marginal models, and conditional models are the three main types of extensions of generalized linear models for longitudinal data, and they make differing assumptions about the joint distribution of the measured responses. Random-effect models [18] assume that a subset of the regression coefficients vary across subjects according to a certain distribution, usually normal. Marginal models can be used to make inferences about population averages, since they model the average response of a sub-population that has the same value for a certain covariate. Parameters of marginal models can be estimated using the generalized estimating equations [19], which do not assume any specific form of the joint distribution of a subject’s measurements, but are based on a quasi-likelihood approach. Conditional models are usually

transition models, where conditional distribution of each response is a function of preceding responses and covariate values [16]. There exist also semiparametric and nonparametric approaches, such as local polynomial and spline methods [20]. Generalized linear mixed models [21], which contain both fixed and random effects have remained a highly used approach. This is because they are an interpretable, fast and powerful model family that usually can be fitted using off-the-shelf software for different types of response variables. The popular R-package *lme4* [12] can be used to fit mixed models using the maximum likelihood or restricted maximum likelihood (REML) method. In practice, however, it is difficult to fit mixed models which involve effects of many crossing categorical covariates, and *lme4* will report a singular fit or imperfect convergence. Hierarchical Bayesian models [22] provide an alternative where the population and group-level parameters have a clearer interpretation, uncertainty can be assessed and posterior diagnostics studied. Their software implementations include *brms* [23, 24] and *rstanarm* [25]. Gaussian process ANOVA [3] is another approach to separate shared effects and interactions of various categorical factors. The *mgcv* package implements generalized additive mixed models [26] based on penalized regression splines.

Longitudinal studies commonly collect many covariates and typically only part of them have an effect on the response. Determining the relevant covariates is a critical research question which can provide important insights about the modeled phenomenon. The covariate relevance information can be used to obtain a better interpretability of the disease development, build models for better predictions and reduce future measurement costs. Despite its importance, the covariate selection aspect for longitudinal data has been largely overlooked. In general, the covariate selection problem is often approached by defining a set of alternative models, and recasting it as a model selection problem. Alternatively, significance of different model terms can be tested in a frequentist manner, but for mixed models it is not straightforward to determine the denominator degrees of freedom when computing p-values [27]. Approaches for model selection for linear mixed models, reviewed in [28], include for example information criteria and shrinkage methods. Bayesian models can be compared by information criteria or cross-validation [10], but in general one would need to perform exhaustive search over different models to select the relevant covariates.

GP is a popular Bayesian nonparametric model that is commonly used for time series modeling [1, 29]. GPs can be made additive by defining an additive kernel function, which provides a flexible yet interpretable model class. Additive GP models can be interpreted analogously with the standard linear mixed models, with the exception that each component in an additive GP model is a flexible nonparametric function. The balance between interpretability and flexibility in time series modeling was initially studied by Plate [30], who proposed to use a sum of univariate and multivariate kernels. An additive kernel that contains all interaction terms was proposed by Duvenaud *et al.* [2] and more complex decomposable additive structures were proposed in [31]. While much of the work on learning GP regression models from data has relied on type-II maximum likelihood estimation, Bayesian techniques have also been proposed in [32, 30, 33]. More recently, semi-parametric models that mix linear, spline and GP components [34] as well as more general additive GPs [35, 36, 37] have been proposed. Additive GP models that are particularly designed for longitudinal study designs include a method of Quintana *et al.* [37] and *LonGP* [4]. *LonGP* uses a stepwise search algorithm for uncovering relevant covariates and was shown to provide accurate covariate selection. However, stepwise search strategies are prone to overfitting at different stages of the search procedure, and the cross-validation based model selection of *LonGP* requires the user to set two different non-trivial threshold values that guide the model search. The stepwise algorithm requires sampling the posterior of GP hyperparameters at each stage, which becomes computationally exhaustive in the presence of many covariates. Furthermore, search algorithms in general will only provide the researcher the information about which model was selected, instead of a relevance measure for all covariates.

Our way of defining the proportion of variance explained by signal is closely related to the recently introduced Bayesian R^2 -statistic [8]. Like our method, it takes into account the problem that the classical definition of R^2 is not suitable for Bayesian models, since the variance of the predicted values

can be larger than the variance of the data. One question that can arise is why not directly use the samples of the kernel hyperparameter α_j^2 to divide the proportion of signal between the model components. While they indeed are informative of the effect sizes, we find that studying the posterior of the function components more clearly distinguishes the relevant components. Also the component lengthscales have been used to determine covariate relevance, in an approach that is usually termed automatic relevance determination (ARD) [38]. The motivation is that smaller lengthscales would indicate more relevant components, but ARD has shown to rather measure nonlinearity than relevance [39]. Recently, decomposing the variance explained by different predictors of general machine learning models has also been approached by computing Shapley values, which have game theoretic basis [40]. Shapley values for each predictor are obtained as a solution to a coalition game, in which predictors have different contributions to the coalition, i.e. the total prediction.

References

- [1] C. E. Rasmussen and C. K. I. Williams, *Gaussian Processes for Machine Learning*. MIT Press, 2006.
- [2] D. K. Duvenaud, H. Nickisch, and C. E. Rasmussen, “Additive Gaussian processes,” in *Advances in Neural Information Processing Systems 24*, 2011.
- [3] C. G. Kaufman and S. R. Sain, “Bayesian functional ANOVA modeling using Gaussian process prior distributions,” *Bayesian Analysis*, vol. 5, no. 1, pp. 123–149, 2010.
- [4] L. Cheng, S. Ramchandran, T. Vatanen, N. Lietzen, R. Lahesmaa, A. Vehtari, and H. Lähdesmäki, “An additive Gaussian process regression model for interpretable non-parametric analysis of longitudinal data,” *Nature Communications*, vol. 10, no. 1, 2019.
- [5] M. D. Hoffman and A. Gelman, “The No-U-Turn Sampler: Adaptively setting path lengths in Hamiltonian Monte Carlo,” *Journal of Machine Learning Research*, vol. 15, no. 1, pp. 1593–1623, 2014.
- [6] M. Betancourt, “A conceptual introduction to Hamiltonian Monte Carlo,” *arXiv:1701.02434*, 2017.
- [7] B. Carpenter, A. Gelman, M. D. Hoffman, D. Lee, B. Goodrich, M. Betancourt, M. A. Brubaker, J. Guo, P. Li, and A. Riddell, “Stan: A probabilistic programming language,” *Journal of Statistical Software*, vol. 76, no. 1, 2017.
- [8] A. Gelman, B. Goodrich, J. Gabry, and A. Vehtari, “R-squared for Bayesian regression models,” *The American Statistician*, vol. 73, no. 3, pp. 307–309, 2019.
- [9] C. Goutis and C. P. Robert, “Model choice in generalised linear models: A Bayesian approach via Kullback-Leibler projections,” *Biometrika*, vol. 85, no. 1, pp. 29–37, 1998.
- [10] J. Piironen and A. Vehtari, “Comparison of Bayesian predictive methods for model selection,” *Statistics and Computing*, vol. 27, no. 3, pp. 711–735, 2017.
- [11] X. Robin, N. Turck, A. Hainard, N. Tiberti, F. Lisacek, J.-C. Sanchez, and M. Müller, “pROC: an open-source package for R and S+ to analyze and compare ROC curves,” *BMC Bioinformatics*, vol. 12, p. 77, 2011.
- [12] D. Bates, M. Mächler, B. Bolker, and S. Walker, “Fitting linear mixed-effects models using lme4,” *Journal of Statistical Software*, vol. 67, no. 1, pp. 1–48, 2015.
- [13] A. Kuznetsova, P. B. Brockhoff, and R. H. B. Christensen, “lmerTest package: Tests in linear mixed effects models,” *Journal of Statistical Software*, vol. 82, no. 13, pp. 1–26, 2017.

- [14] C.-W. Liu, L. Bramer, B.-J. Webb-Robertson, K. Waugh, M. J. Rewers, and Q. Zhang, “Temporal expression profiling of plasma proteins reveals oxidative stress in early stages of type 1 diabetes progression,” *Journal of Proteomics*, vol. 172, pp. 100–110, 2018.
- [15] A. Vehtari, A. Gelman, D. Simpson, B. Carpenter, and P.-C. Bürkner, “Rank-normalization, folding, and localization: An improved \hat{R} for assessing convergence of MCMC,” 2019.
- [16] P. Diggle, P. Heagerty, K.-Y. Liang, and S. Zeger, *Analysis of Longitudinal Data*. Oxford University Press, 2002.
- [17] G. M. Fitzmaurice, N. M. Laird, and J. H. Ware, *Applied longitudinal analysis*. Wiley-Interscience Hoboken, N.J, 2004.
- [18] N. M. Laird and J. H. Ware, “Random-effects models for longitudinal data,” *Biometrics*, vol. 38, no. 4, p. 963–974, 1982.
- [19] K.-Y. Liang and S. L. Zeger, “Longitudinal data analysis using generalized linear models,” *Biometrika*, vol. 73, no. 1, pp. 13–22, 1986.
- [20] H. Wu and J.-T. Zhang, *Nonparametric Regression Methods for Longitudinal Data Analysis: Mixed-effects Modeling Approaches*. Wiley, 2006.
- [21] G. Molenberghs and G. Verbeke, “A review on linear mixed models for longitudinal data, possibly subject to dropout,” *Statistical Modeling*, 2001.
- [22] A. Gelman and J. Hill, *Data Analysis Using Regression and Multilevel/Hierarchical Models*. Cambridge University Press, 2006.
- [23] P.-C. Bürkner, “brms: An R package for Bayesian multilevel models using Stan,” *Journal of Statistical Software*, vol. 80, no. 1, 2017.
- [24] P.-C. Bürkner, “Advanced bayesian multilevel modeling with the R package brms,” *The R Journal*, vol. 10, no. 1, pp. 395–411, 2018.
- [25] Stan Development Team, “rstanarm: Bayesian applied regression modeling via Stan,” 2016. R package version 2.13.1.
- [26] S. Wood, *Generalized additive models: an introduction with R*. Texts in Statistical Science, UK United Kingdom: Chapman & Hall, 2006.
- [27] S. G. Luke, “Evaluating significance in linear mixed-effects models in R,” *Behavior Research Methods*, vol. 49, no. 4, pp. 1494–1502, 2017.
- [28] S. Müller, J. L. Scaely, and A. H. Welsh, “Model selection in linear mixed models,” *Statistical Science*, vol. 28, pp. 135–167, 2013.
- [29] S. Roberts, M. Osborne, M. Ebden, S. Reece, N. Gibson, and S. Aigrain, “Gaussian processes for time-series modelling,” *Philosophical Transactions of the Royal Society A: Mathematical, Physical and Engineering Sciences*, vol. 371, no. 1984, p. 20110550, 2013.
- [30] T. A. Plate, “Accuracy versus interpretability in flexible modeling: implementing a tradeoff using Gaussian process models,” *Behaviormetrika*, vol. 26, pp. 29–50, 1999.
- [31] D. Duvenaud, J. Lloyd, R. Grosse, J. Tenenbaum, and G. Zoubin, “Structure discovery in nonparametric regression through compositional kernel search,” in *Proceedings of the 30th International Conference on Machine Learning* (S. Dasgupta and D. McAllester, eds.), vol. 28 of *Proceedings of Machine Learning Research*, (Atlanta, Georgia, USA), pp. 1166–1174, PMLR, 2013.

- [32] R. M. Neal, “Monte carlo implementation of Gaussian process models for Bayesian regression and classification,” *arXiv:physics/9701026*, 1997.
- [33] E. Gilboa, Y. Saatçi, and J. P. Cunningham, “Scaling multidimensional inference for structured gaussian processes,” *IEEE Transactions on Pattern Analysis and Machine Intelligence*, vol. 37, no. 2, pp. 424–436, 2015.
- [34] P. Schulam and S. Saria, “A framework for individualizing predictions of disease trajectories by exploiting multi-resolution structure,” in *Proceedings of the 28th International Conference on Neural Information Processing Systems - Volume 1, NIPS’15*, (Cambridge, MA, USA), pp. 748–756, MIT Press, 2015.
- [35] S. Qamar and S. T. Tokdar, “Additive Gaussian Process Regression,” *arXiv:1411.7009*, 2014.
- [36] G. Vo and D. Pati, “Sparse additive gaussian process with soft interactions,” *Open Journal of Statistics*, vol. 7, no. 4, 2017.
- [37] F. A. Quintana, W. O. Johnson, L. E. Waetjen, and E. B. Gold, “Bayesian nonparametric longitudinal data analysis,” *Journal of the American Statistical Association*, vol. 111, no. 515, pp. 1168–1181, 2016.
- [38] R. M. Neal, *Bayesian Learning for Neural Networks*. PhD thesis, University of Toronto, 1995.
- [39] T. Paananen, J. Piironen, M. R. Andersen, and A. Vehtari, “Variable selection for Gaussian processes via sensitivity analysis of the posterior predictive distribution,” in *Proceedings of Machine Learning Research*, vol. 89 of *Proceedings of Machine Learning Research*, pp. 1743–1752, PMLR, 16–18 Apr 2019.
- [40] N. Redell, “Shapley Decomposition of R-Squared in Machine Learning Models,” *arXiv:1908.09718*, Aug 2019.

A Proof of the zero-sum property

Theorem 1.

Let $r \in \{1, \dots, M\} = \mathcal{M}$, where $M \geq 2$. We define a kernel function

$$k_{\text{zerosum}}(r, r' | M) = \begin{cases} 1 & \text{if } r = r' \\ -\frac{1}{M-1} & \text{otherwise} \end{cases}. \quad (26)$$

Let $k_{\text{base}} : (\mathcal{X}, \mathcal{X}) \rightarrow \mathbb{R}$ be another kernel function. Furthermore, we denote their product kernel by $k = k_{\text{zerosum}}k_{\text{base}}$. Now assume that function $f : (\mathcal{X}, \mathcal{M}) \rightarrow \mathbb{R}$ has GP prior $f \sim \mathcal{GP}(0, k)$. Then for any $t \in \mathcal{X}$, the prior distribution of the sum $g(t) = \sum_{r=1}^M f(t, r)$ is the Dirac delta distribution at zero.

Proof.

We study the product kernel in the limit $k = \lim_{\epsilon \rightarrow 0^+} k_\epsilon$, where

$$k_\epsilon(\mathbf{x}, \mathbf{x}') = k(\mathbf{x}, \mathbf{x}') + \epsilon \cdot \mathcal{K}(\mathbf{x}, \mathbf{x}'), \quad (27)$$

and $\mathcal{K}(\mathbf{x}, \mathbf{x}')$ is one if the inputs are the same data point, and 0 otherwise. Assume that f has GP prior $f \sim \mathcal{GP}(0, k_\epsilon)$ and $\epsilon > 0$. For any fixed $t \in \mathbb{R}$, we have $\mathbf{f}_t \sim \mathcal{N}(0, \mathbf{K}_\epsilon)$, where

$$\mathbf{f}_t = \begin{bmatrix} f(t, 1) \\ \vdots \\ f(t, M) \end{bmatrix} \quad \text{and} \quad \mathbf{K}_\epsilon = \begin{bmatrix} k_{\text{base}}(t, t) + \epsilon & & -\frac{k_{\text{base}}(t, t)}{M-1} \\ & \ddots & \\ -\frac{k_{\text{base}}(t, t)}{M-1} & & k_{\text{base}}(t, t) + \epsilon \end{bmatrix}. \quad (28)$$

Since $g(t) = \sum_{r=1}^M f(t, r) = \mathbf{1}^\top \mathbf{f}_t$, we get

$$g(t) \sim \mathcal{N}(\mu, \sigma_\epsilon^2), \quad (29)$$

where $\mu = \mathbf{1}^\top \mathbf{0} = 0$ and $\sigma_\epsilon^2 = \mathbf{1}^\top \mathbf{K}_\epsilon \mathbf{1} = M \cdot \epsilon$. Therefore, the limit distribution of $g(t)$ is

$$\lim_{\epsilon \rightarrow 0^+} \mathcal{N}(0, \sigma_\epsilon^2) = \lim_{\epsilon \rightarrow 0^+} \mathcal{N}(0, M \cdot \epsilon) = \delta_0, \quad (30)$$

i.e. the Dirac delta distribution.

Corollary.

With any data, also the posterior distribution of $g(t)$ is δ_0 .

B Figures S1-S8

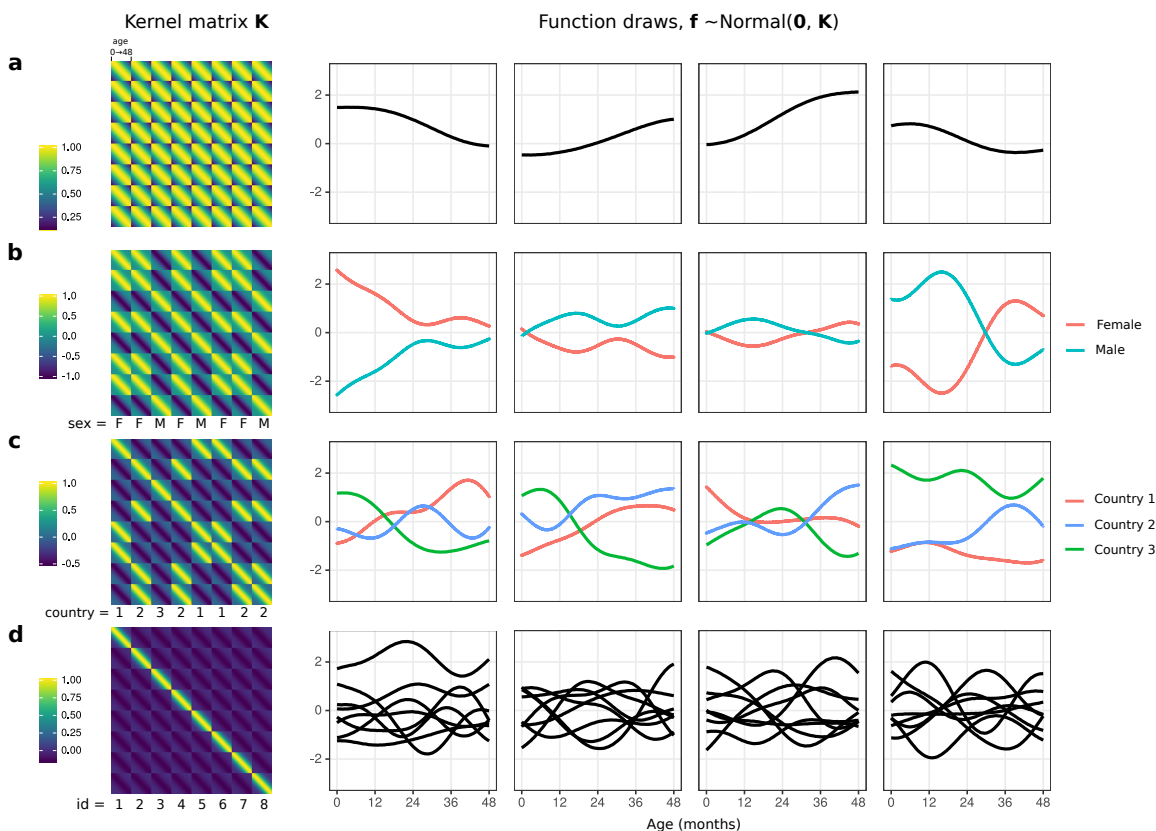


Figure S1. Illustration of the zero-sum kernel for modeling category-specific time-dependent deviations from a shared age profile. Each row shows a kernel matrix and four randomly drawn function realizations for 8 individuals on age span 0 to 48 months. Marginal standard deviation $\alpha = 1$ has been used for all kernels. **a)** A standard squared exponential kernel for modeling shared age effects, with lengthscale 24 months. **b)** The new zero-sum kernel with two categories (Female, Male) and lengthscale 12 months. **c)** A zero-sum kernel with three categories (Country 1, Country 2, Country 3) and lengthscale 12 months. **d)** A zero-sum kernel with 8 categories ($\text{id} = 1, \dots, 8$) and lengthscale 12 months, for modeling individual-specific time-dependent deviations from the shared age profile.

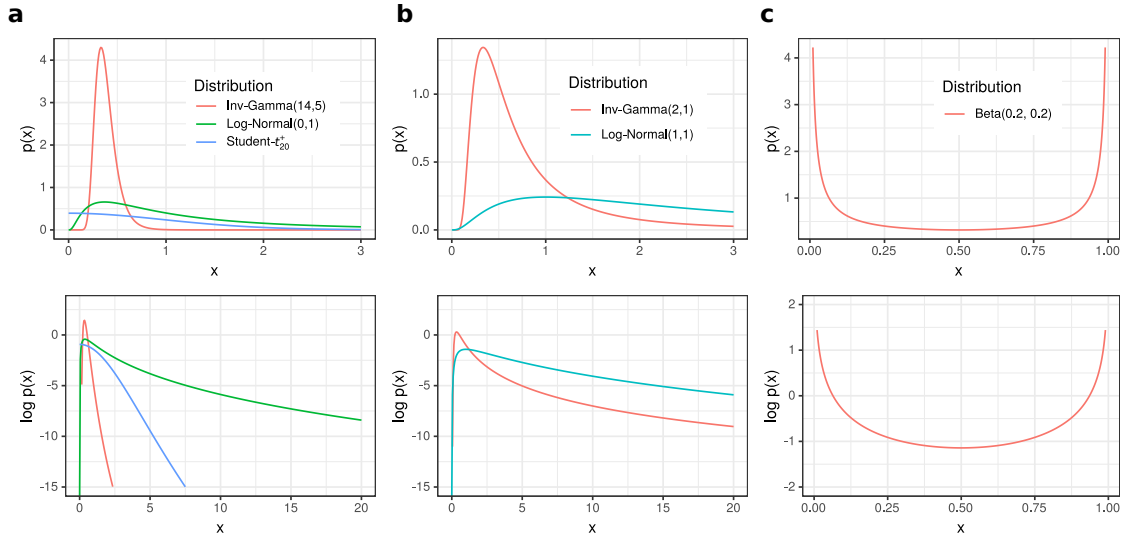


Figure S2. Visualization of the prior distributions used for model parameters. Top row shows probability density functions of the distributions and bottom row shows the corresponding densities on log-scale. **a)** Prior distributions for kernel function parameters. A half Student- t prior is used for the marginal standard deviation parameters α , because it has a long tail but its mode is at zero. A log-normal prior is suitable for the lengthscales ℓ because it does not allow values near zero. An inverse gamma distribution is used for the input warping steepness parameter a . **b)** Prior distributions for likelihood function parameters. An inverse gamma distribution is used for the noise variance parameter σ_n^2 when using a Gaussian likelihood model. A log-normal prior is used for the inverse overdispersion parameter ϕ of the negative binomial distribution. **c)** A beta prior for the individual-specific disease effect magnitude parameters is used to prefer parameter values close to either zero or one. Here the beta distribution density is plotted at points $0.01 \leq x \leq 0.99$.

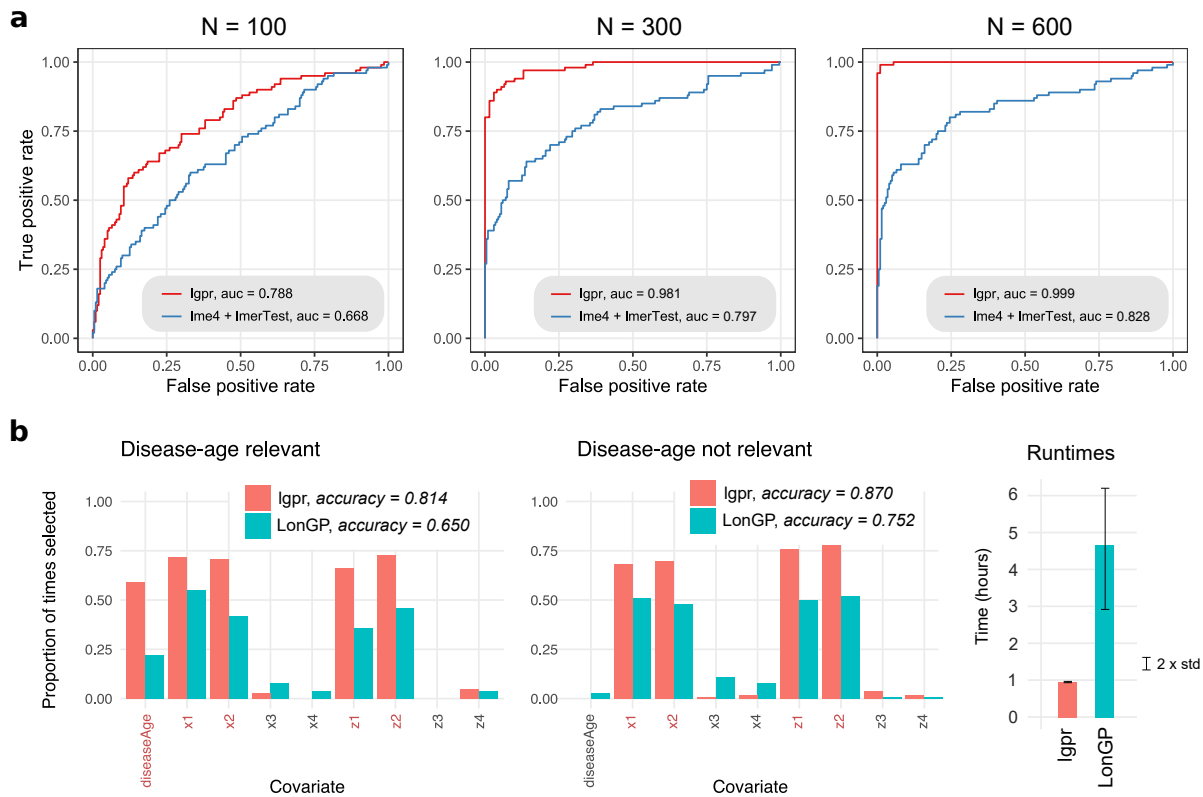


Figure S3. Covariate selection accuracy of lgpr is superior to previous methods. **a)** Comparison with linear mixed effect modeling and demonstration of our method’s scalability. The panels show ROC curves for the problem of classifying covariates as relevant or irrelevant, when the total number of data points is $N = 100$, 300 and 600, respectively. **b)** Comparison against *LonGP* in the task of selecting relevant covariates. The bar plots show the fraction of times each covariate was chosen in the final model over 100 simulated data sets. Red text indicates the covariates that were relevant in generating the data. The left panel shows results for 100 simulations that includes the disease-related age (*diseaseAge*) as a relevant covariate. The center panel shows results for 100 simulations where the disease-related age was not a relevant covariate. The right panel shows distribution of runtimes over the total 200 simulations for both methods. The bar lengths are average runtimes, and the turnstiles indicate runtime standard deviations.

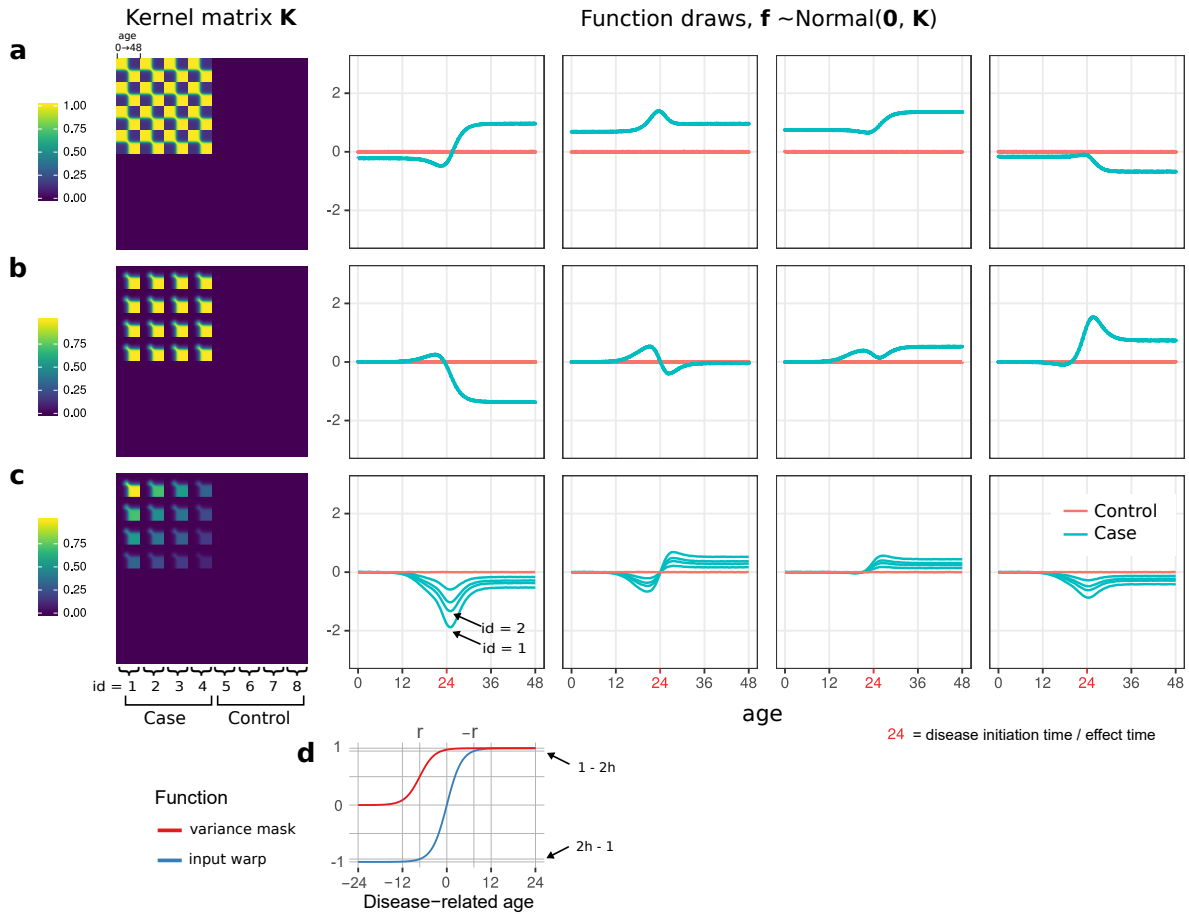


Figure S4. Illustration of different kernels for modeling a non-stationary disease effect. Each row shows a kernel matrix and four randomly drawn function realizations for 8 individuals (4 case, 4 control) on age span 0 to 48 months. Marginal standard deviation $\alpha_{\text{diseaseAge}} = 1$, lengthscale $\ell_{\text{diseaseAge}} = 1$ and warping steepness $a = 0.5$ have been used for all kernels and the disease effect time is at 24 months. **a)** Standard non-stationary kernel using the input warping approach. The input warping allows the function to vary in time only near the disease effect time for cases, but also allows a baseline difference between cases and controls. **b)** The new variance masked kernel, which does not allow any difference between groups until close to the effect time and after it. **c)** Heterogeneous version of the variance masked kernel, which in addition allows the magnitude of the disease effect to differ between case individuals. Individual-specific disease effect magnitude parameters have been set to $\beta_1 = 1, \beta_2 = 0.5, \beta_3 = 0.3, \beta_4 = 0.1$. **d)** The input warping and variance masking functions.

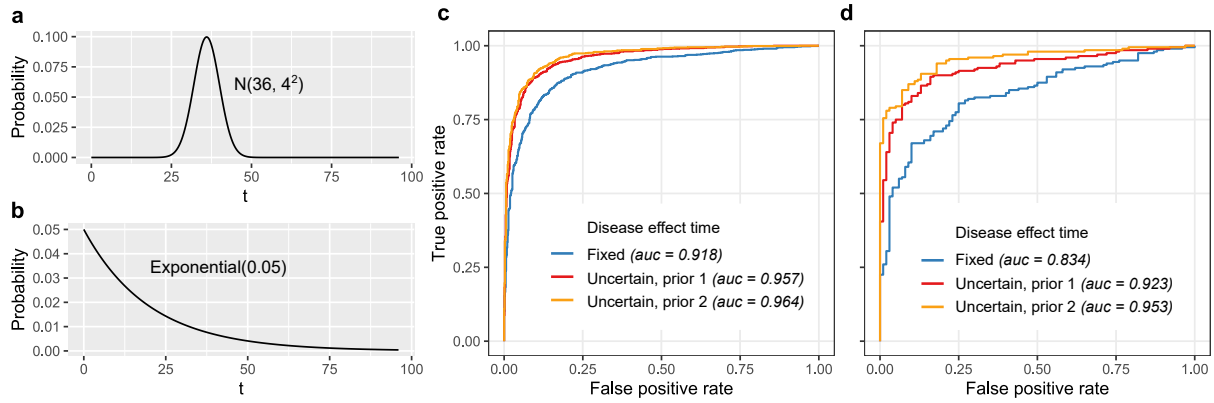


Figure S5. Modeling the uncertainty in the disease effect time enhances covariate selection accuracy. Results of an experiment where data is simulated so that the disease effect can occur earlier than the observed disease initiation. **(a)** The distribution from which the real effect time for each diseased individual is sampled from. **(b)** The distribution from which the disease detection delay is sampled from. **(c)** ROC curves for covariate selection with and without modeling the effect time uncertainty. The yellow curve is for a model where the prior of effect time was the same as the distribution in **(a)** (*prior 1*). The red curve is for a model with an exponential decay prior for the difference between the effect time and observed onset (*prior 2*). The blue curve is for a model with effect time fixed to equal the observed initiation time. **(d)** ROC curves for the same three models, in the task of classifying just the disease component as relevant or irrelevant.

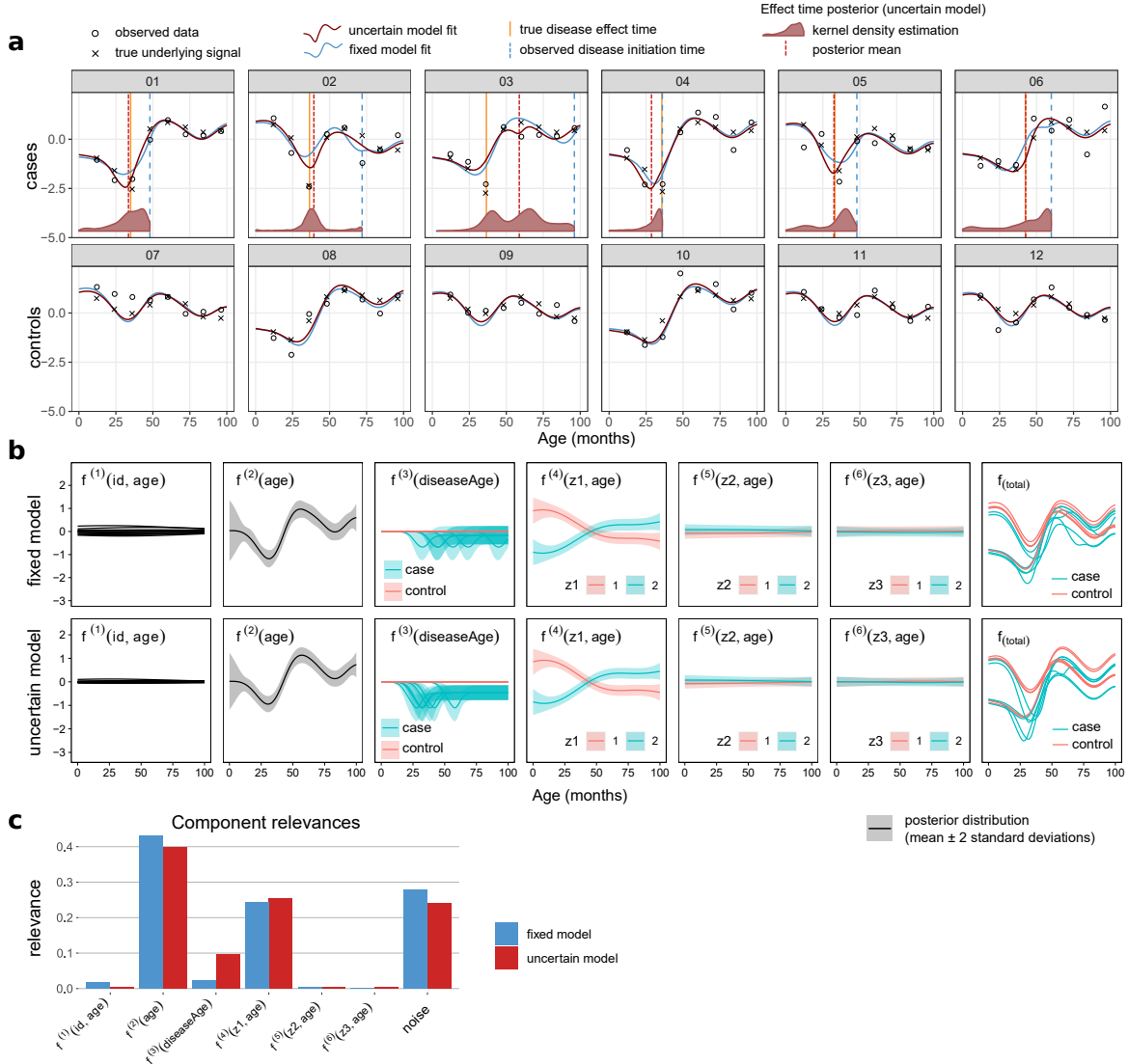


Figure S6. Demonstration of inferring the uncertain disease effect time using simulated data. a) The data-generating process, noisy data and fits of the uncertain and fixed models plotted for each of the 12 individuals. The fixed model uses the observed disease initiation time (dashed blue line), whereas the uncertain model infers it from data. The uncertain model can more clearly identify the disease effect, because disease initiation is observed later than the true effect occurrence (yellow line). Model fits are the posterior predictive means, computed using posterior mean parameters. **b)** Posterior distributions of each inferred function component for both models, using posterior mean parameter values. For clarity, standard deviations are not shown for $f^{(1)}$ and $f_{(\text{total})} = \sum_{j=1}^6 f^{(j)}$. **c)** Component relevances inferred by both models for this data realization. The true relevant components were $f^{(2)}$, $f^{(3)}$ and $f^{(4)}$. The simulated data was generated as explained in Section 3.4, except with signal-to-noise ratio 3.

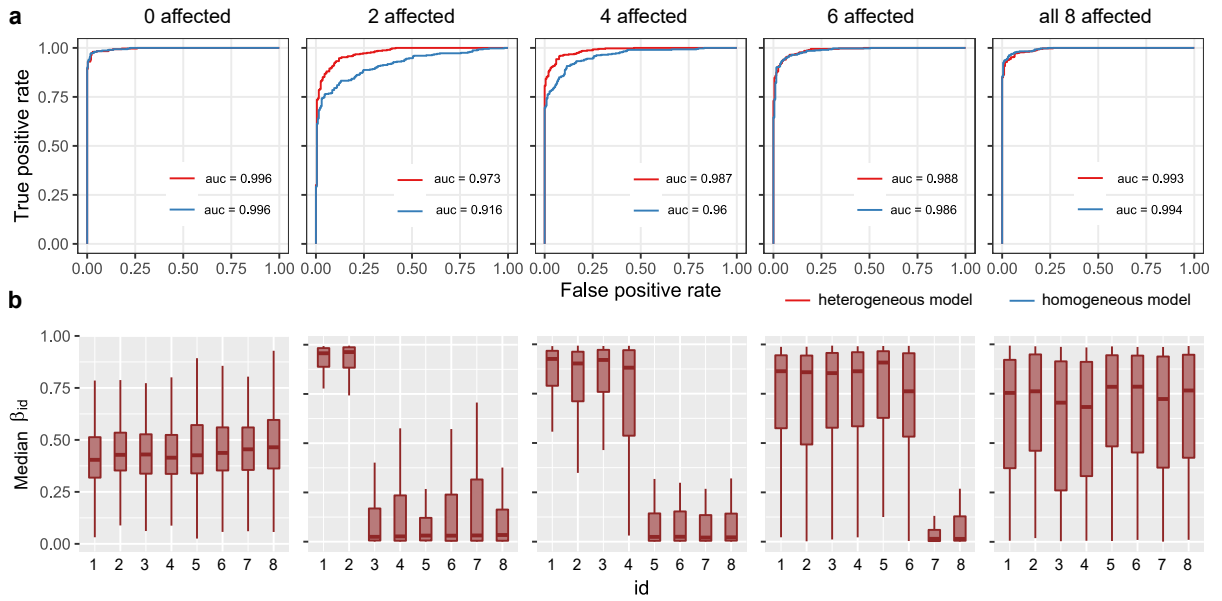


Figure S7. Heterogeneous modeling of the disease effect is beneficial when only some of the diagnosed individuals are affected by the disease. **a)** The ROC curves for covariate selection using a heterogeneous and a homogeneous disease model in the simulated data experiments with 0, 2, 4, 6 and 8 out of the 8 diagnosed individuals affected, respectively. **b)** Inferring the individual-specific disease effect magnitude parameters can reveal the individuals affected by the disease. The boxplots show the distributions of the posterior medians of β_{id} , $id = 1, \dots, 8$ of the heterogeneous model, over 100 simulated data sets. The box is the interquartile range (IQR) between the 25th and 75th percentiles, vertical line inside the box is the 50th percentile, and the whiskers extend a distance of at most $1.5 \cdot IQR$ from the box boundary. Each panel corresponds to the same experiment as the one above it.

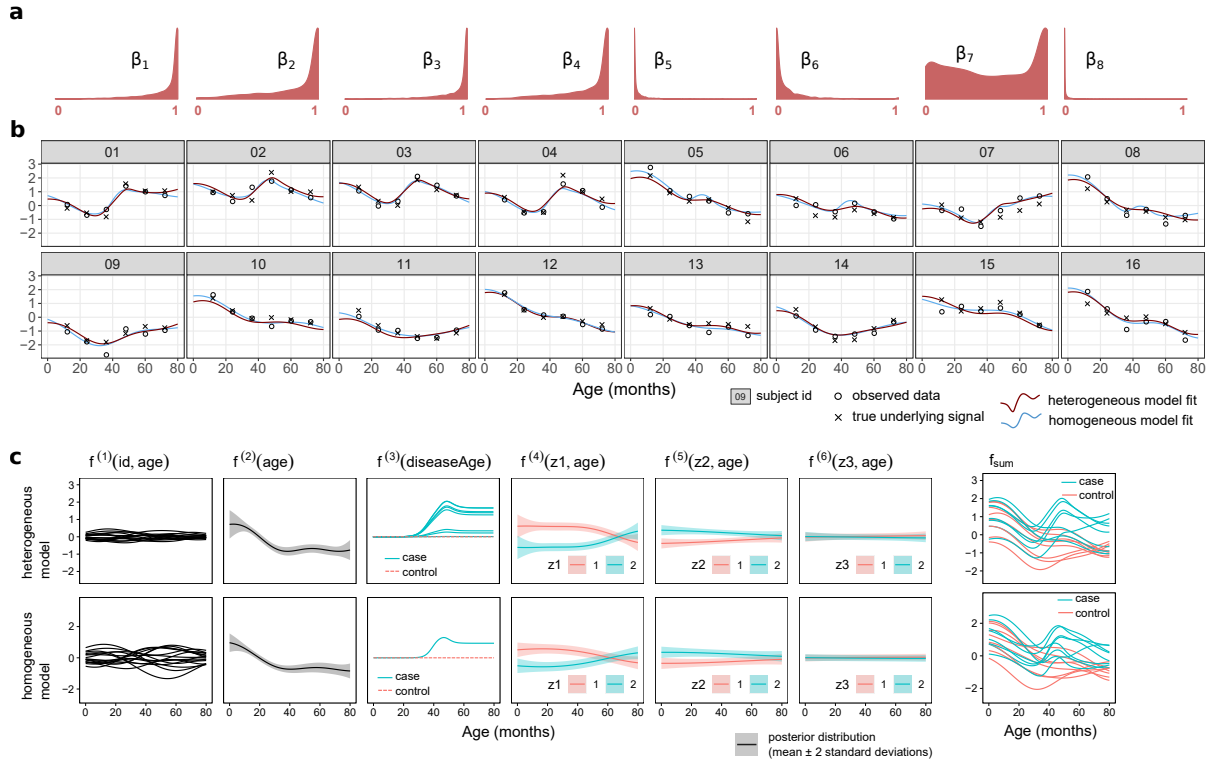


Figure S8. Demonstration of inferring a heterogeneous disease effect using simulated data. Individuals 01-08 are cases, but the disease effect is generated only for individuals 01-04. **a)** Kernel density estimates for the posteriors of the individual-specific disease effect magnitude parameters β_{id} , $\text{id} = 1, \dots, 8$. **b)** The data-generating process, noisy data and fits of the heterogeneous and homogeneous models plotted for each of the 16 individuals separately. Model fits are the posterior predictive means, computed using maximum a posterior (MAP) parameter values. **c)** Posterior distributions of each inferred function component for both models, using MAP parameter values. For clarity, standard deviations are not shown for $f^{(1)}$, $f^{(3)}$ and $f_{\text{sum}} = \sum_{j=1}^6 f^{(j)}$. The true relevant components were $f^{(2)}$, $f^{(3)}$ and $f^{(4)}$. The simulated data was generated as explained in Section 3.3, except with signal-to-noise ratio 5.